Dielectric Polymers for High-Temperature Capacitive Energy Storage

He Li,[†a,b,c] Yao Zhou,[†a] Yang Liu,[a] Li Li,[a] Yi Liu*[b,c] and Qing Wang*[a]

Polymers are the preferred materials for dielectrics in high-energy-density capacitors. The electrification of transport and growing demand for advanced electronics require polymer dielectrics capable of operating efficiently at high temperatures. In this review, we critically analyze the most recent development in the dielectric polymers for high-temperature capacitive energy storage applications. While general design considerations are discussed, emphasis is placed on the elucidation of the structural dependence of the high-field dielectric and electrical properties and the capacitive performance, including discharged energy density, charge–discharge efficiency and cyclability, of dielectric polymers at high temperatures. Advantages and limitations of current approaches to high-temperature dielectric polymers are summarized. Challenges along with future research opportunities are highlighted at the end of this article.

1. Introduction

The significant demand for efficient, low-cost and environmentally friendly electrical energy storage technologies is spurred by numerous applications ranging from advanced microelectronics to electric vehicles and grid-connected renewable energy systems.[1–7] Among the current electrical energy storage devices, batteries and electrochemical capacitors based on electrochemical reactions operate under low voltages (*e.g.*, < 5 V) and exhibit considerably higher energy densities (*e.g.*, 900–2500 J cm^{-3} of lithium-ion batteries, 200–400 J cm^{-3} of lead-acid batteries and 20–29 J cm^{-3} of commercial electrochemical capacitors)[7–14] than dielectric capacitors (*e.g.*, < 5 J cm^{-3} at 700 MV m^{-1} of biaxially-oriented polypropylene, BOPP, which is the industrial benchmark dielectric polymer).[15–17] On the other hand, dielectric capacitors that store electrical energy in an electrostatic field possess the highest power densities, *i.e.*, up to 10^7–10^8 W kg^{-1} versus 10^1–10^2 W kg^{-1} of batteries and 10^2–10^6 W kg^{-1} of electrochemical capacitors, owing to their fastest charge–discharge rates at a micro-second scale.[18–22] Dielectric capacitors are thus essential for pulsed power applications such as electrified transportation, power conditioning and switching, and advanced propulsion.[15,23–25]

As shown in Fig. 1, dielectric polymer film capacitors comprise ~50 percent of the global high voltage capacitor market.[26] Compared to ceramic capacitors,[27–31] polymer film capacitors exhibit more than one order of magnitude higher breakdown strength (*i.e.*, MV m^{-1}), thereby giving rise to great energy densities and high reliability.[32–38] Moreover, the unique graceful failure mechanism allows reliable operation of dielectric polymers at high electric fields.[39–41] Additionally, polymer dielectrics possess a series of intrinsic advantages including lightweight, low cost, mechanical flexibility, robust charging–discharging cyclability and facile large-scale processability.[41–46]

On the other hand, dielectric polymers are more vulnerable to extreme temperatures and consequently have much lower working temperatures in comparison to their ceramic counterparts, *e.g.*, BOPP operates at temperatures < 105 °C under applied electric fields, which fail to meet the rising demand for capacitive energy storage under the extreme conditions present in the applications as illustrated in Fig. 1.[25,28,47–49] For instance, dielectric capacitors are currently used in inverters of hybrid and electric vehicles to control and convert direct current (DC) from batteries into alternating current (AC) required to drive the motor, where the temperature is around 140–150 °C.[50,51] Similarly, aircraft electrification requires the power converters to be located in or near turbine engines where the working temperature ranges from 180–300 °C.[52] The rapid evolution of wide bandgap semiconductors, *e.g.*, silicon carbide and gallium nitride, necessitates the efficient operation of power electronics with integrated capacitors at temperatures well above 150 °C.[53,54] The working temperatures of the sensing electronics and electric compressors used in underground oil and gas exploration are in the range of 170−300 °C depending on the drill depth.[55] Therefore, to accommodate BOPP in high-temperature power electronics, *e.g.*, the inverters in Toyota

[a] *Department of Materials Science and Engineering, The Pennsylvania State University, University Park, Pennsylvania, 16802 USA. E-mail: wang@matse.psu.edu*
[b] *Materials Sciences Division, Lawrence Berkeley National Laboratory, Berkeley, California, 94720 USA. E-mail: yliu@lbl.gov*
[c] *Molecular Foundry, Lawrence Berkeley National Laboratory, Berkeley, California, 94720 USA.*
† *H.L. and Y.Z. contributed equally to this work.*

Prius® hybrid electric vehicles, a secondary cooling system has been employed to reduce the local maximum temperature (*e.g.*, 140–150 ℃) to 65–70 ℃.[16,47,56] Unfortunately, the additional cooling loop brings extra mass and volume to power electronic systems and reduces fuel efficiency.[47,57]

For capacitive energy storage applications, dielectric properties including dielectric constant (K), dissipation factor (tan δ), dielectric breakdown strength (E_b) and electrical conductivity play important roles in determining capacitive performance, *i.e.*, discharged energy density (U_e) and charge–discharge efficiency (η), of dielectric materials. Specifically, K is associated with the inherent capacity of a dielectric for electrostatic charge storage while E_b determines the maximum electric field that a dielectric can withstand during the charging process. In addition, tan δ and electrical conductivity govern the energy loss of dielectric materials, both of which are expected to be as low as possible for capacitor dielectrics. Polymers usually display strong temperature dependence of dielectric properties especially where the thermal transition occurs such as at the glass transition temperature (T_g). Engineering aromatic polymers with high T_g values have been developed as high-temperature dielectric materials to address the imperative needs shown in Fig. 1.[25,47,48,58–60] Indeed, under weak electric fields, the engineering polymers such as polycarbonate (PC, T_g ~150 ℃), polyetherimide (PEI, T_g ~ 217 ℃), fluorene polyester (FPE, T_g ~330 ℃) and polyimide (PI, T_g ~ 360 ℃) exhibit highly stable K and tan δ values with respect to temperature up to their respective T_g.[6,47] Unfortunately, this design strategy has had only limited success when applied to high-temperature dielectric polymers operating at high electric fields. Under high applied electric fields, the engineering polymers typically show substantially reduced E_b, decreased U_e and much lowered η values with increasing temperature, even when the temperature is well below their T_g. For example, the U_e and the η of capacitor-grade Kapton® PI decline precipitately from 1.53 J cm^{-3} and 95.2%, respectively, at room temperature to 0.6 J cm^{-3} and 21.8% as temperature rises to 150 ℃.[61]

The sharply reduced capacitive performance of dielectric polymers with increasing temperature is mainly attributed to the exponential increase of leakage current activated by thermal and electric fields. For instance, the electrical conductivity of Kapton® PI shows almost two orders of magnitude increases when the applied field is increased from 50 MV m^{-1} to 250 MV m^{-1} at 150 °C, *i.e.*, from 6.8×10^{-13} S m^{-1} to 3.5×10^{-11} S m^{-1}. Comparatively, at room temperature, PI has a conductivity of 4.4×10^{-15} S m^{-1} at 50 MV m^{-1}.[6,61,62] Note that the increase of conduction and the decrease of electrical resistivity of polymers with the applied field and temperature is a general phenomenon.[6,47,63] For example, Fig. 2 summarizes the changes in the current density and the DC electrical resistivity of polypropylene (PP) and low-density polyethylene (LDPE) with the increase of the electric field and temperature.[64–66]

Therefore, the improvement of the high-temperature capacitive performance of dielectric polymers via suppressing conduction at elevated temperatures and high applied fields is fundamentally challenging. Recently, breakthrough results have been achieved by using wide bandgap inorganic fillers to inhibit charge injection and conduction in polymers.[6,61,67–75] The resulting dielectric polymer composites exhibit remarkable capacitive performance at high temperatures, far exceeding the current dielectric polymers. Different from prior reviews covering the high-temperature dielectric polymer composites,[47,48,58,59,76–79] this article exclusively focuses on the recent innovations in all-organic dielectric polymers that are designed for capacitive energy storage applications at high electric field and high temperature (*i.e.*, ≥ 200 MV m^{-1} and ≥ 120 °C). The structure-property correlation and the guidelines for the structural design of high-temperature polymer dielectrics are summarized and discussed.

The review starts with the description of the fundamentals of dielectric properties, capacitive performance and the graceful failure mechanism of dielectric polymers. The strategies include the design of polymer backbone structures, the dipolar grafting modification approach, the crosslinking chemistries for thermoset and thermoplastic polymers, and the all-organic multicomponent polymers. The last section of this article provides concluding remarks followed by viewpoints regarding challenges and opportunities for the future developments of high-temperature capacitive polymers.

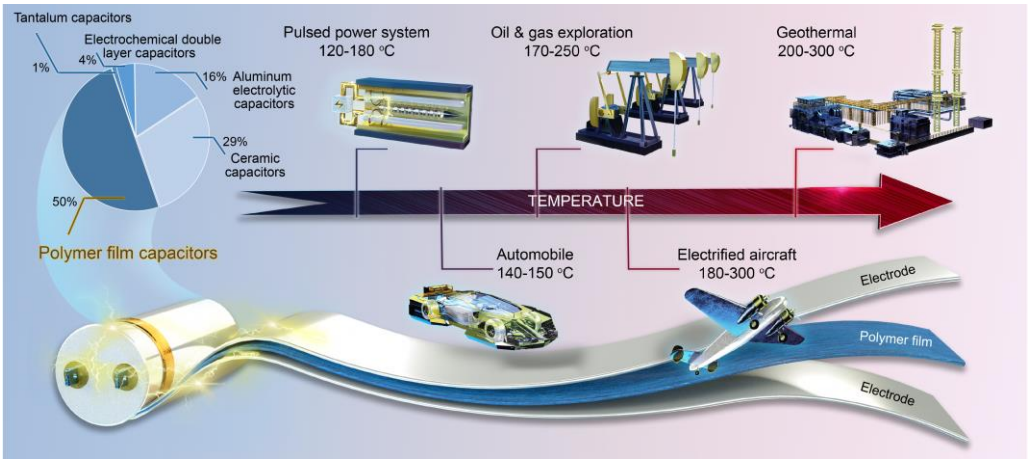

Fig. 1 Market share of the global high-voltage capacitors and the applications of high-temperature dielectric polymer film capacitors.[26]

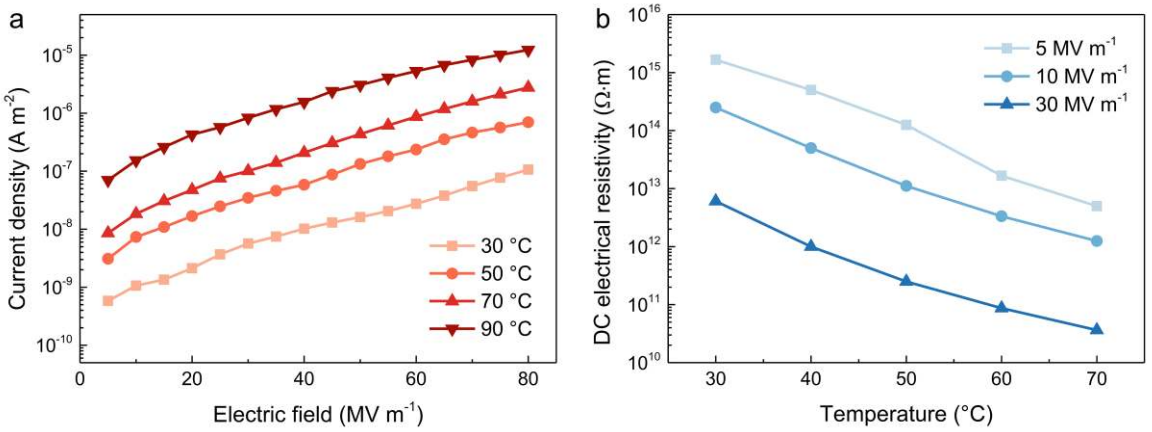

Fig. 2 (a) Current density of PP,[64] and (b) electrical resistivity of LDPE at various electric fields and temperatures.[65] Reproduced from ref. 64 and ref. 65 with permission from IEEE.

2. Electrical properties, capacitive performance and graceful failure modes of polymers

2.1. Electrical polarization and dielectric properties

The electrical polarization is defined as the total dipole moments in a dielectric per unit volume. The degree of polarization is related to the K of the dielectric material and the applied electric field E, which can be expressed as $P = (K - 1)\varepsilon_0 E$, where P is the polarization and ε_0 is the permittivity of vacuum (*i.e.*, 8.85×10^{-12} F m^{-1}).[80] There are four main types of polarization in dielectric materials, which are divided based on the resonance and relaxation regimes, *i.e.*, electronic, ionic, dipolar (orientational) and interfacial (space charge) polarizations (Fig. 3a).[81] For polymer dielectrics, the polarization is closely related to the molecular chain movement and also the frequency of the applied electric field. Consequently, the dielectric response of polymer dielectrics shows typical temperature- and frequency-dependent characteristics.

The electronic polarization is associated with the displacement of the electrons with respect to the nucleus under the applied electric field as shown in Fig. 3b.[82] For solid polymer dielectrics with covalent bonds, the electronic polarization from the core electrons is quite small and the main polarization comes from the valence electrons.[83] Ionic polarization occurs in ionic materials, as illustrated in Fig. 3c.[82] The electronic and ionic polarizations are within the resonance optical and infrared frequency range, respectively. Because of the ultra-high frequencies, there is no dielectric loss in either the electronic or ionic polarization. Both the electronic and ionic polarizations are temperature dependent and exhibit positive temperature coefficients.[83] To improve the electronic polarization, electrons should be delocalized. However, the delocalization of electrons would result in the reduction of the bandgap of polymeric materials. In order to induce high ionic polarization, carbon can be replaced by other group 14 elements (such as silicon) to make ions more dynamic in polymers.[84]

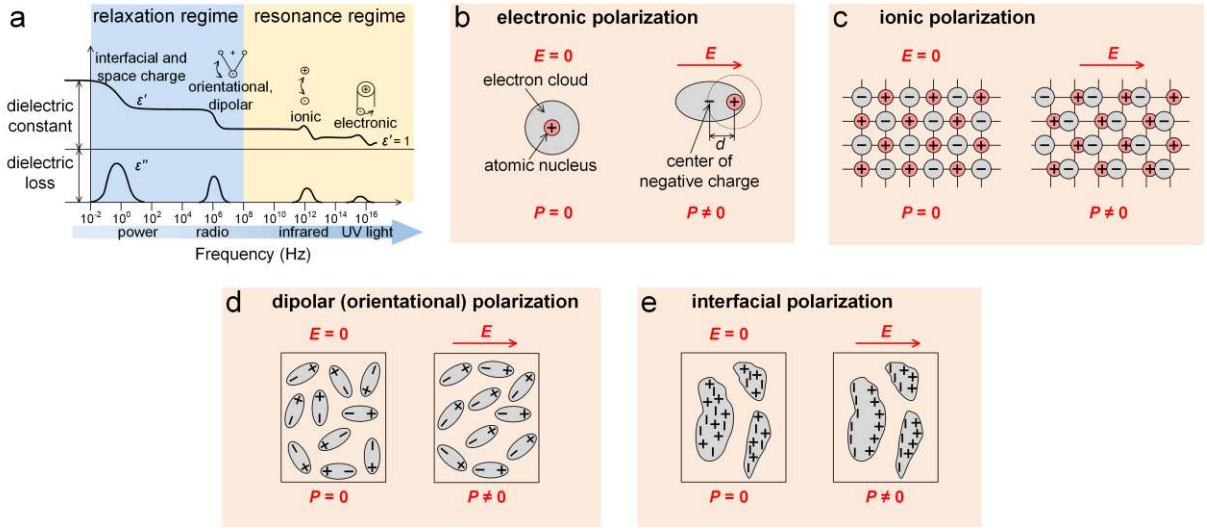

Fig. 3 (a) Frequency-dependent polarization types.[81] Schematic of (b) electronic polarization, (c) ionic polarization, (d) dipolar (orientational) polarization and (e) interfacial polarization.[82] Reproduced from ref. 81 with permission from American Chemical Society and ref. 82 with permission from Elsevier.

The dielectric properties of polymers are significantly influenced by their polarity. The electronic and ionic polarizations that respond at high frequencies are instantaneous. As a result, the K in this region is usually small for both polar and nonpolar polymers. The dipolar (orientational) polarization plays an important role in determining the K of polymer materials and exists in polar materials with permanent dipoles (Fig. 3d).[82] As dipoles need energy to overcome the resistance from the nearby dipoles, the dipolar (orientational) polarization would cause energy loss and is also temperature-dependent.[83] With the increase of temperature, the dipole mobility and consequently the dipolar (orientational) polarization increase. However, with further increasing temperature, the increased thermal movement of the molecules would hinder the dipole orientation, thereby reducing the polarization. The dipolar (orientational) polarization falls into the relaxation regime and usually occurs in the radio frequency range. As a result, the dipolar (orientational) polarization is also frequency-dependent, *i.e.*, the polarization decreases with frequency increase because the dipole orientation cannot catch up with the frequency of the applied electric field.

Interfacial polarization, also known as Maxwell-Wagner-Sillars polarization,[82] appears because of the accumulated charges at the interface between two regions in dielectrics, particularly for heterogeneous materials, such as dielectric polymer composites (Fig. 3e).[85] In polymer dielectrics, various factors, including material non-homogeneity, the presence of impurities, the crystal/amorphous interfaces and the incomplete contact between dielectric films and electrodes, may lead to interfacial polarization. The interfacial polarization occurs at very low frequencies. To utilize the interfacial polarization, polymer composites with high-K fillers and multi-layered polymer films were proposed.[6,44,86] For the multi-layered polymer films, the interfacial polarization exists at the interface between different layers owing to the large contrasts in K and conductivity.

For polymer dielectrics, two types of dielectric losses are presented, *i.e.*, the frequency-independent Ohmic conduction loss which is due to the long-range movement of charges and the frequency-dependent loss associated with energy absorption to move the charges with the electric field.[87] There are usually two types of dipolar relaxations in dielectric polymers, *i.e.*, dipolar segmental relaxation associated with the motion of the whole chain (known as the α relaxation), and dipolar group relaxation associated with the localized motion of the molecules as well as small chain units (known as the β and γ relaxation).[88] The β relaxation corresponds to the relaxation of the side groups, conformational flip of cyclic unit or local motion of the dipolar group across the main chain. The γ relaxation is related to the movements of small units of the main chain or side chain, which occurs at a much lower temperature. Maintaining a low dielectric loss is important for dielectric materials, particularly for capacitors. The dielectric loss builds up equivalent series resistance (ESR) coupled with the capacitor, which contributes to Joule heating in high-current circuitries and is detrimental to capacitors.[56]

Since the polarization and relaxation of the charges and dipoles are dependent on both temperature and frequency, the K and tan δ are influenced by temperature and electric field frequency. For capacitor applications, the variation of the K should be minimized under different operation conditions. Polymers are known to display large variations in K and tan δ when the temperature approaches the T_g.[88] Therefore, polymers with high T_g are considered as candidates for elevated-temperature dielectric applications.[47] However, it should be noted that the tan δ only represents the dielectric loss at low electric fields. When used as high-temperature capacitive material which is subjected to both high temperatures and large applied electric fields, the high-T_g polymers have had limited success because the energy loss under high temperatures and high electric fields mainly comes from the sharply increased conduction loss. Therefore, T_g is only a prerequisite for the design of high-temperature polymer dielectrics, but it does not guarantee desirable capacitive performance at elevated temperatures.

2.2. Dielectric breakdown strength

The dielectric breakdown strength (E_b) is one of the governing parameters that determine the electrostatic energy storage density of dielectric materials. The dielectric breakdown mechanisms are complicated and strongly depend on the material composition, electrical conductivity, thermal conductivity, film thickness, and temperature and electrical stress conditions. Among the different dielectric breakdown mechanisms, free volume breakdown, thermal breakdown and electromechanical breakdown are most likely to occur under high temperature conditions.[89]

Free volume breakdown is an electronic breakdown process in which electrons are accelerated by the applied electric field and the high-energy-electrons would attack the polymer chain to induce the initial breakdown process.[89] The considerable increase of the free volume when temperature approaches T_g necessitates the design of high-temperature polymer dielectrics with high T_g. Crosslinking is commonly adopted to reduce the free volume and increases the E_b of polymers at high temperatures.

For soft dielectric materials such as polymers, the thickness of the material can be reduced due to the Maxwell electrostatic stress under high electric fields, giving rise to the so-called electromechanical breakdown.[89] The electromechanical breakdown electric field can be given as, $E_b = 0.606\left(\frac{Y}{\varepsilon_r \varepsilon_0}\right)^{0.5}$, where Y is the Young's modulus. Since the elastic modulus of polymer materials decreases at high temperatures, especially near the softening temperatures, such as T_g and melting temperature (T_m), the electromechanical breakdown mechanism is applicable to many polymer dielectrics in high temperature regions.[89,90] Note that in a practical film capacitor winding, the inner layers actually don't experience the electrostatic stress, only the outer layer does.

When operating under both high electric field and high temperature conditions, the electrical conductivity of polymer dielectrics increases sharply due to various electric field- and temperature-dependent conduction mechanisms. As a result of Joule heating from the increased conductivity, the internal temperature of the dielectric material increases. On the other hand, heat dissipation in polymer dielectrics is rather difficult as polymers usually have relatively low thermal conductivities.[91] If heat generation exceeds the rate of heat loss, the temperature of dielectric materials would continue to rise, which in turn leads to a further increase in heat generation and eventually the so-called thermal breakdown.[92] The heat equilibrium during the thermal breakdown process can be expressed as, $C_v \frac{\partial T}{\partial t} = \sigma(E,T)E^2 + \nabla \cdot (\lambda(T)\nabla T)$, where C_v is the specific heat at constant volume, σ is the electrical conductivity, λ is

the thermal conductivity, T is temperature. Obviously, simply increasing T_g cannot effectively increase the thermal breakdown strength. It is thus more important to suppress electrical conductivity under high electric fields and elevated temperatures, which is particularly important for the design of high-temperature polymer dielectrics.

It should be noted that although many breakdown theories have been proposed, it is still challenging to distinguish which mechanism predominates the dielectric breakdown process of polymer dielectrics because the dielectric breakdown of polymers strongly depends on various factors, such as temperature, voltage ramp, film thickness, electrical stress, electrical conduction, thermal conduction and material defects.[89,93] It requires comprehensive investigation and also case-by-case analysis to clarify the dielectric breakdown mechanism. Moreover, the measured breakdown field also highly relies on the effective electrode area of a dielectric material because the effective area of the electrode is proportional to the defect probability of dielectric film samples, which deserves careful consideration on the evaluation of novel dielectric for potential capacitor applications.

The Weibull statistics is widely used to evaluate the dielectric breakdown data. The two-parameter Weibull distribution can be expressed as, $P(E)=1-\exp\left(-\left(E/E_b\right)^{\beta}\right)$, where $P(E)$ is the cumulative probability of dielectric breakdown, E is the measured breakdown strength, E_b is the characteristic breakdown strength which corresponds to 63.2% probability of breakdown, and the shape parameter β evaluates the scatter of data.[93]

2.3. Electrical conduction

The electrical conduction of polymer dielectric is not only related to the intrinsic properties of the polymers, but also closely depends on temperature and applied electric field. Under high electric fields and high temperatures, significant leakage current occurs in polymer dielectrics, including those occurring in the bulk of the dielectrics and at the dielectric/electrode interface.[94] The high leakage current is the main cause of the large increase in energy loss under high electric fields and high temperatures, which is fundamentally different from the dielectric loss measured from dielectric spectroscopy. The high leakage current also leads to undesirable temperature rise inside the polymer dielectrics and consequently thermal runaway of the film capacitors. Generally, the electrical conduction current of polymers can be written as, $J=ne\mu E$, where J is the conduction current density, n is the charge carrier density, e is the electron charge, μ is the charge carrier mobility. Under low electric fields, it can be considered that n and μ are only affected by temperature. Therefore, the conduction mechanism is Ohmic conduction, where the conduction current increases linearly with the applied electric field. However, as the applied electric field increases, n and μ are significantly affected by the electric field, and the conduction current deviates from the Ohm's law and increases with the electric field nonlinearly. With the increase of temperature, more charge carriers would be thermally activated to participate in the electrical conduction and the charge carrier mobility also increases. Therefore, the conduction current of polymer dielectrics typically shows exponential growth with temperature.[63,91] For example, the electrical conductivity of cross-linked polyethylene (XLPE, which is commonly used in insulation for high voltage power cables) measured at an electric field of 10 MV m^{-1} increases from 1.47 x 10^{-16} S m^{-1} at 30 °C to 5.08 x 10^{-14} S m^{-1} at 90 °C.[95] As shown in Fig. 4, various conduction mechanisms have been proposed, including hopping conduction, Poole-Frenkel emission, Schottky emission and field emission.

Hopping conduction usually occurs in the bulk of semicrystalline polymer dielectrics (Fig. 4a). With the increase of temperature and electric field, the charge carriers could gain more energy to jump over the potential barriers established between the short-range ordered domains by long-range disordered structures in polymers, resulting in sharply increased conduction current.[96] The hopping conduction current density J_H can be expressed as, $J_H=2ne\lambda\nu\exp\left(-\frac{\mu_H}{kT}\right)\sinh\left(\frac{\lambda eE}{2kT}\right)$, where λ is the hopping distance, ν is the attempt-to-escape frequency, μ_H is the barrier height and k is the Bolzmann constant. To suppress the hopping conduction current, the hopping barrier height should be increased and the hopping distance should be decreased, *e.g.*, introducing more deep charge traps.

For polymer dielectric materials, charge traps exist due to the physical and chemical defects. The decreased potential barrier of the charge traps upon the increase of the applied field allows more constrained charge carriers to overcome the potential barrier and participate in the conduction process (Fig. 4b), giving rise to the so-called Poole-Frenkel emission conduction mechanism.[97] The conduction current density of Poole-Frenkel emission J_{PF} can be expressed as, $J_{PF}=\sigma_0 E\exp\left(-\frac{\mu_{PF}}{kT}\right)\exp\left(\frac{\sqrt{e^3/\pi\varepsilon_0\varepsilon_r}\sqrt{E}}{kT}\right)$, where σ_0 is the conductivity under low electric fields and μ_{PF} is the barrier height of charge traps. The Poole-Frenkel emission is closely related to the trap energy level in polymer dielectrics. Increasing the trap energy level is beneficial to suppress the Poole-Frenkel emission conduction.

Due to the different band structures, the energy barrier exists at the metal electrode/polymer dielectric interface. The charge carriers from the electrode must overcome this energy barrier to be injected into the polymer dielectrics (Fig. 4c). With the increase of temperature, charge carriers gain sufficient energy from thermal activation to overcome the energy barrier at the electrode/polymer interface and increase the conduction current, which is called as thermionic emission. Moreover, the presence of a high electric field can further assist the charge carrier emission by decreasing the energy barrier at the electrode/polymer interface, which further increases the conduction current. This is the so-called electric field-assisted thermionic emission, which is also known as Schottky emission.[98] The Schottky emission conduction current density J_S can be expressed as, $J_S=AT^2\exp\left(-\frac{\phi}{kT}\right)\exp\left(\frac{\sqrt{e^3/4\pi\varepsilon_0\varepsilon_r}\sqrt{E}}{kT}\right)$, where A is the Richardson constant and ϕ is the electrode/dielectric barrier height. To suppress the Schottky emission conduction current, the energy barrier at the electrode/polymer interface should be increased, *e.g.*, embedding a carefully selected charge blocking layer between the electrode and polymer dielectric. Apart from the thermal activation, charge carriers can obtain energy directly from the applied high electric fields at ambient and even lower

temperatures to overcome the energy barrier, which is called field emission conduction.[99] The field emission conduction current density J_F can be expressed as, $J_F = \frac{AT^2\pi \exp\left(-2\alpha\phi^{3/2}/3eE\right)}{\left(\alpha\phi^{1/2}kT/eE\right)\sin\left(\pi\alpha\phi^{1/2}kT/eE\right)}$ and $\alpha = \frac{4\pi\sqrt{2m}}{h}$, where m is the effective electron mass, h is the Planck constant.

The above-mentioned conduction mechanisms indicate that the electrical conduction in polymer dielectrics is much more significant at high temperatures than that at room temperature. The temperature has an even greater impact on electrical conduction under high electric fields due to the field-dependent effect. Accordingly, the conduction current of polymer dielectrics increases dramatically under elevated temperatures and high electric fields, thus greatly increasing the probability of thermal runaway. Therefore, suppressing the conduction current is of vital importance for the design of polymer dielectrics for high-temperature capacitive applications, which is different from the polymer dielectrics operating at room temperature.

2.4. Capacitive performance

The capacitive energy storage performance of dielectric materials is related to the applied electric field and the polarization response induced by the electric field. In general, the volumetric charged energy density (U_s) of a dielectric material can be written as, $U_s = \int_{D_{max}}^{0} E\mathrm{d}D$ and $D = \varepsilon_0 E + P = \varepsilon_0 KE$, where D is the electric displacement induced by the electric field and P is the electric polarization. For linear dielectrics, such as the nonpolar polymers, the K is independent on the applied electric field. U_s can be written as, $U_s = \frac{1}{2}DE = \frac{1}{2}\varepsilon_0 KE^2$. Clearly, in order to obtain high U_s, high K, and more importantly, high E_b are desired as U_s is proportional to the square of E.[100]

U_e can be calculated from the electric displacement–electric field (D–E) loops by the integral of the shaded area bounded by the discharging curve (Fig. 5). Fig. 5a and b show the typical D–E loops of linear and nonlinear dielectrics. Note that the D–E loop in Fig. 5a is an ideal case, actually, even linear dielectrics may have hysteresis-like dielectric response under high electric fields and elevated

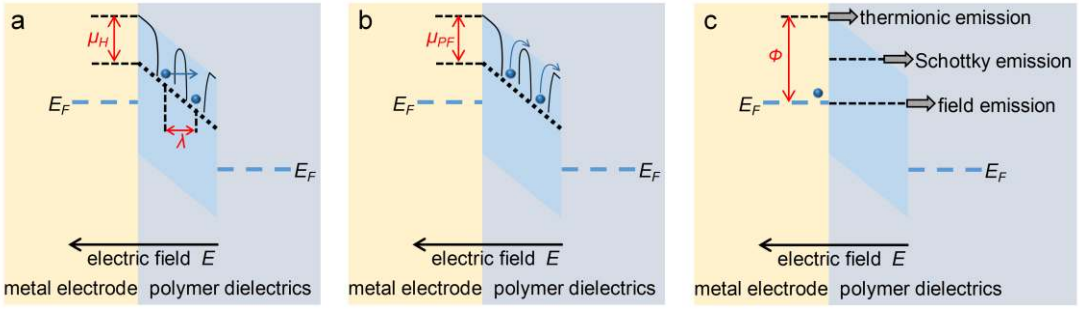

Fig. 4 Schematic of (a) hopping conduction, (b) Poole-Frenkel emission, and (c) thermionic emission, Schottky emission and field emission.[94] Reproduced from ref. 94 with open access from Hindawi.

temperatures due to the inevitable conduction loss. Ferroelectric materials with a D–E loop shown in Fig. 5c have larger polarization than normal dielectrics and are potentially a class of dielectric materials with higher energy densities. However, the ferroelectric loss caused by the remnant polarization generates substantial energy loss. By decreasing the ferroelectric domain size and the energy barrier in the phase transition, normal ferroelectrics can be converted into relaxor ferroelectrics (Fig. 5d), leading to reduced hysteresis loss and improved η at room temperature.[101] However, there still exists large conduction loss in relaxor ferroelectrics at high temperatures.

It is noteworthy that U_e is not equal to U_s because of the presence of various energy loss mechanisms, including conduction loss, polarization loss and hysteresis loss. Considering the energy loss, η, calculated from $\eta = U_e/U_s$, is another key parameter to evaluate the capacitive performance. The energy that cannot be fully released is converted into waste heat, which may lead to the aging and thermal runaway of dielectric materials. Although linear polymer dielectrics are often viewed as ideal insulators with negligible or extremely low conduction loss at room temperature,[6,17,25] they often show poor η under high temperatures and high electric fields, which is due to the sharply increased electrical conduction attributed to various temperature- and electric field-dependent conduction mechanisms.[6] Again, suppression of the conduction loss under high temperatures and high electric fields is beneficial to improving η and U_e.

As discussed in Section 2.2, the effective electrode area of the dielectric material largely affects the E_b value which would further influence the U_s value. Similarly, the energy loss of the dielectric material derived from D–E loop measurement is also highly dominated by the applied frequency, *e.g.*, the lower applied frequency offers more time for dipole to orient under electric field, which would undoubtedly contribute more energy loss compared to the measurements conducted under higher frequencies. Therefore, the leading parameters such as E_b, η and U_e of a dielectric film sample may differ under different test conditions. To provide the readers with a more intuitive comparison, we summarized the key physical parameters and measurement conditions including electrode area, test frequency and film thickness of the high-temperature dielectric polymers in Table 1.

2.5. Commercially available polymers for film capacitors

BOPP is the state-of-the-art commercial dielectric polymers, especially for high voltage and high frequency applications. PP, a nonpolar polymer shown in Fig. 6a, possesses excellent electrical resistance and high breakdown strength of ~700 MV m^{-1} at room

temperature.[16,17] Moreover, the K (~2.25 at 1 kHz) and tan δ (~0.01% at 1 kHz) of BOPP are essentially frequency-independent at temperatures below 100 ℃. The U_e of BOPP is maximized to ~5 J cm^{-3} at room temperature and an electric field of 700 MV m^{-1}. The maximum operating temperature for the BOPP capacitor is about 105 ℃ with appropriate voltage derating, which is mainly caused by the sharply increased electrical conductivity at high temperatures. For example, the DC volume electrical resistivity of BOPP measured at an applied field of 200 MV m^{-1} decreases from 6.04 x 10^{14} Ω·m to 2.53 x 10^{11} Ω·m with the increase of temperature from 20 ℃ to 120 ° C .[17] As compared in Fig. 6b, the U_e and η decrease constantly from 2.43 J cm^{-3} and 99.3% at room temperature to 2.00 J cm^{-3} and 80.5% at 100 °C and 1.28 J cm^{-3} and 52.1% at 120 °C, respectively, under an applied electric field of 500 MV m^{-1}.[17] More seriously, although BOPP almost shows no deterioration of capacitive performance in consecutive charging–discharging cycles at room temperature under 200 MV m^{-1}, which is the operation field of film capacitors in electric vehicles, the increasing temperature not only decreases the U_e and η but also brings raising concerns with regards to operating reliability. For example, the BOPP was broken down around 10 200 cycles at 120 °C and 200 MV m^{-1}.[17]

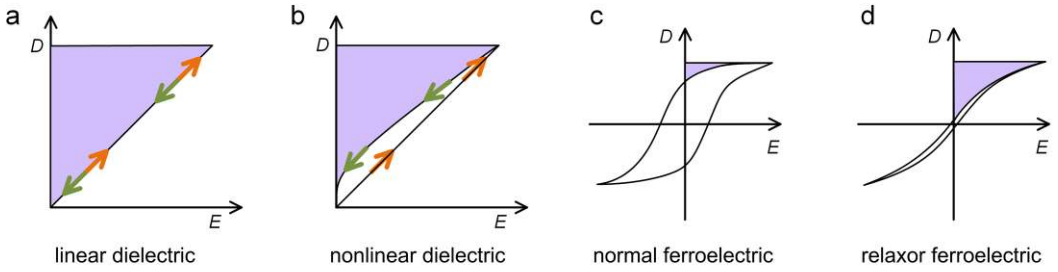

Fig. 5 Schematic of *D*–*E* loops of (a) unipolar for linear dielectrics, (b) unipolar for nonlinear dielectrics, (c) bipolar for normal ferroelectrics and (d) bipolar for relaxor ferroelectrics.[102] Reproduced from ref. 102 with permission from American Chemical Society.

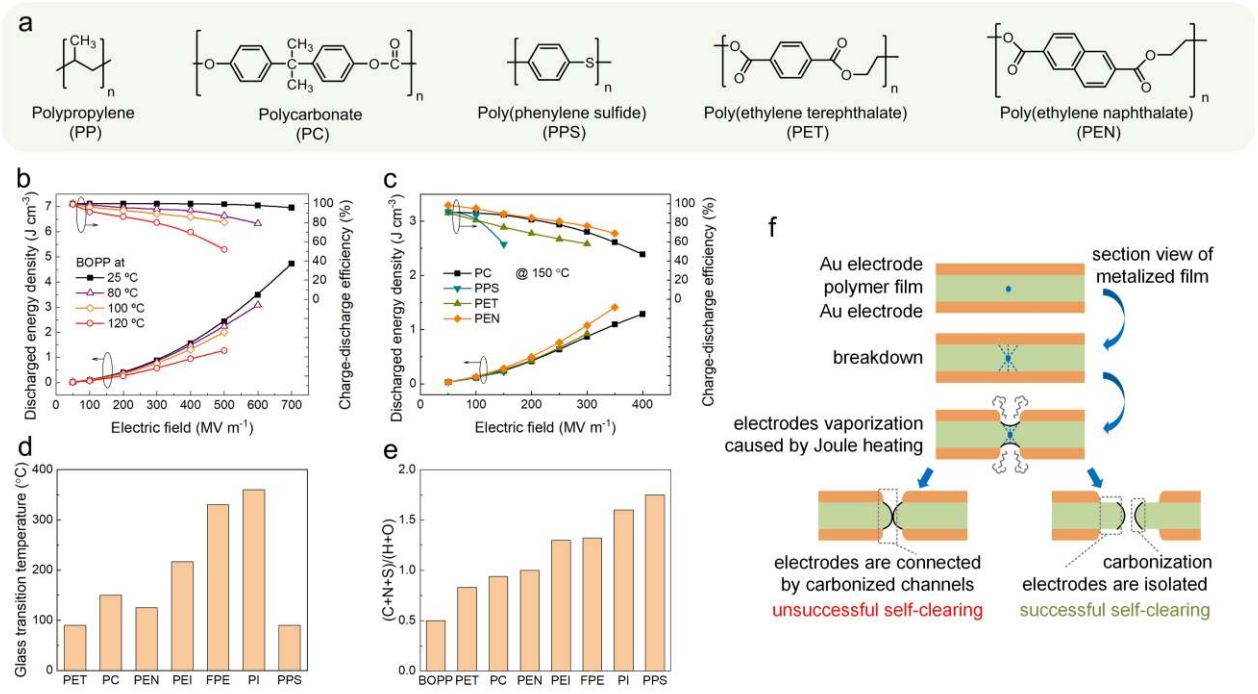

Fig. 6. (a) Chemical structures of PP, PC, PPS, PET and PEN. (b) Discharged energy density and charge–discharge efficiency of BOPP at varied temperatures. (c) Discharged energy density and charge–discharge efficiency of PC, PPS, PET and PEN at 150 °C.[17] (d) Glass transition temperature and (e) The ratio of (carbon + nitrogen + sulfur) to (hydrogen + oxygen) of high-temperature dielectric polymers. (f) Schematic of the self-clearing process.[104] Reproduced from ref. 17 with permission from John Wiley and Sons and from ref. 104 with permission from Elsevier.

To date, a variety of high-T_g engineering polymers have been explored and commercialized as high-temperature film capacitor dielectrics as shown in Fig. 6a, including PC, poly(phenylene sulfide) (PPS), poly(ethylene terephthalate)

(PET), poly(ethylene 2,6-naphthalate) (PEN). The capacitive energy storage properties measured at 150 ℃ of these high-temperature dielectric polymers are summarized in Fig. 6c. The T_g values of these high-temperature polymers along with that of the aforementioned PEI, FPE and PI are depicted in Fig. 6d.[48]

PC, a bisphenol A-based aromatic polymer synthesized from carbonic acid and dihydric alcohols, is mostly in the amorphous phase and has a T_g of around 150–160 ºC. PC possesses a K of about 3 with high stability over temperature, *e.g.*, the temperature coefficient of the capacitance is only 2% at 125 ℃, and a low tan δ of 0.1% at 1 kHz from 25 ℃ to 125 ºC.[6] At 150 ℃, PC exhibits an U_e of 1.29 J cm^{-3} and a η of 47% at 400 MV m^{-1}. Since 2000, Bayer AG, the main supplier of PC, discontinued the production and the market share of PC film capacitors dropped precipitately. PPS, with aromatic rings linked by sulfides, has been regarded as an excellent substitute for PC in high-temperature capacitors because of a similar K (*i.e.*, ~3–3.1) as well as a low tan δ of 0.3% at 1 kHz.[25] However, its poor breakdown strength at elevated temperatures (*e.g.*, 150 ℃, see Fig. 6c) limits the further improvement in U_e. Notably, even though the T_g of PPS is only about 90 ℃, it can be used up to temperatures higher than T_g (*e.g.*, 120 ℃) because of its high crystallinity of 60–65% and a high T_m of 285 ºC. PET, a copolymer of ethylene glycol and terephthalic acid, exhibits a comparable K (~3 at 1 kHz) to PC and PPS.[103] However, the major drawback of PET is the strong temperature dependence of both K and tan δ. Also, the tan δ of PET is fairly large, *i.e.*, 0.2–1% from room temperature to 125 ℃, compared with other high-temperature polymers. Because of the similar polyester structures of PET and PEN, PEN shows a similar temperature-dependent K and tan δ to PET.[103] At 150 ℃, the energy storage performance of PEN is better than that of PET, probably due to its higher T_g (*i.e.*, 125 °C *vs.* 70–80 °C of PET). For example, the U_e and η of PEN are 1.08 J cm^{-3} and 77%, compared to 0.93 J cm^{-3} and 58% of PET, respectively, at 150 °C and 300 MV m^{-1}. Other dielectric polymers with high T_g, including PI (~360 °C) and PEI (~217 °C) represented by the imide ring-based backbone and FPE (~330 °C) with a rigid heterocyclic structure are systematically described in Section 3.2.3 and 3.2.4.

Although these high-T_g polymers show good temperature stability of K, they only work well under relatively low electric fields (*i.e.*, < 200 MV m^{-1}) at high temperatures (*i.e.*, ≥ 120 ℃) and have had very limited success when the polymers are subject to both high temperatures and high electric fields because of high electrical conduction loss and the resulting low η (Fig. 6c).

2.6. Graceful failure mechanism of dielectric polymers

For practical film capacitor applications, large-area dielectric polymer film is metallized with a thin layer of metal as electrodes. In this configuration, the metallized layer functions as a fuse when a localized breakdown of the film occurs during operation.[104,105] As demonstrated in Fig. 6f, an instantaneous surge current flowing through the breakdown site can damage the polymer film by generating intensive Joule heat, which is prone to result in the vaporization or oxidation of metal electrodes on the surface of films. When the freshly exposed area between upper and lower electrodes is large enough to insulate the carbonized perforations around the breakdown site, the capacitor is still able to operate continuously at a full rated voltage, merely at the expense of a small reduction in capacitance. This smart function of metallized films to clear a breakdown site by the energy released in the dielectric breakdown process is the so-called self-clearing, which largely determines the service reliability of dielectric polymer film capacitors.[40] The graceful failure mechanism is a unique characteristic of dielectric polymers. Numerous studies regarding the polymer physics and chemistry of clearing mechanism have been carried out, suggesting that the self-clearing capability mostly depends on the metallization resistivity of the electrodes and the chemical composition of the polymers.[106–108] However, there is currently no universal theory to reveal the direct correlation between the chemical composition and self-clearing ability of dielectric polymers. It is proposed that poor self-clearing often occurs in the polymers with a high ratio of carbon to (hydrogen + oxygen), which generates free carbon to form the conductive path during the film breakdown.[109,110] Conversely, the polymers contain a low ratio of carbon to (hydrogen + oxygen) typically clear themselves well. Fig. 6e presents the ratio of (carbon + nitrogen + sulfur) to (hydrogen + oxygen) of the aforementioned dielectric polymers. The self-clearing capability of other dielectric polymers containing the elements such as fluorine and chlorine other than carbon, hydrogen, oxygen, nitrogen and sulfur also call for in-depth evaluation.

3. Rational design of backbone structures of high-temperature dielectric polymers

In terms of chemical structure, the vast majority of heat-resistant dielectric polymers with high thermo-electrical and -mechanical stability rely on a large number of aromatic groups and/or fused-ring heterocyclic configurations on the backbone, while a few benefit from high crystallinity with little or no aromaticity.

3.1. Aliphatic dielectric fluoropolymers

Most aliphatic polymers have a relatively low T_g (*e.g.*, < 120 °C) and are in a rubber state at the service temperatures of high-temperature capacitors (*e.g.*, ≥ 140 °C), where strong chain segment motion contributes to a large amount of energy loss.[44,48] The crystalline phase of dielectric polymers can effectively inhibit the movement of molecular chains so that aliphatic polymers with high crystallinity, *e.g.*, PP, can withstand operating temperatures higher than their T_g (*i.e.*, < 0 °C).[111]

Polytetrafluoroethylene (PTFE) is a class of nonpolar aliphatic polymer with a fluorine-containing backbone structure and has a T_g of around 115 °C. Known as "The King of Plastic", PTFE was discovered by Plunkett in 1938 and has been widely used above 200 °C in numerous industrial applications owing to its excellent heat resistance up to 260 °C.[48,112] PTFE (Teflon® grade) possesses excellent arc and tracking resistance in air as well as an ultralow tan δ < 0.02% across a wide frequency range from 60 Hz to 3 GHz.[113,114] However, due to the highly crystalline structure with a solid-phase transition temperature of around 325 °C (PTFE has no defined T_m), PTFE has a very high melt viscosity on the order of 10^{10} Pa·s, which leads to difficulties in melt-processing into thin films with thickness less than < 10 μm.[115–117] The PTFE films prepared from sintering solution-dispersed PTFE powders and skiving from a sintered PTFE bulk are prone to contain pinholes and impurity dopants, which raises reliability concerns for long-term high-voltage operation.[117,118]

Teflon® perfluoroalkoxy (PFA), which is a copolymer of tetrafluoroethylene and perfluoroalkyl vinyl ethers, displays better melt-processability when compared to PTFE and a slightly lower T_m of about 305 °C.[119] The K of PFA is around 2.15 at 1 kHz, which maintains fairly stable with the frequency between 50 Hz and 100 kHz measured at 22 ℃ as well as with temperature ranging from 22–200 ℃ at 60 Hz. The PFA film with a typical thickness of 25 μm exhibits an E_b of ~350 MV m^{-1} at 22 ℃, which declines to 320 MV m^{-1} and 245 MV m^{-1} at 125 ℃ and 250 ℃, respectively.[120]

Recently, the field of PTFE-based thin films has witnessed tremendous progress, including the optimization of synthetic approaches and the improvement of the film manufacturing process. For example, a series of new PTFE resins were developed by Gore with greatly improved processability into below 10-μm thin films, presumably by melt-extrusion rather than the conventional dispersing or skiving techniques.[121,122] Impressively, the 6-μm Gore PTFE film exhibits a high E_b than BOPP with the same thickness at 40 ℃ (*i.e.*, 756 MV m^{-1} *vs.* 706 MV m^{-1}) under the same electrode configuration and test condition. Kerwien *et al*. compared the spatial progression of the breakdown sites on a large area (~58 cm^2) of PTFE and BOPP thin films (Fig. 7a-d).[122] It was found that starting from the occurrence of the 1st breakdown event, the breakdown evolution speed of BOPP is faster than that of PTFE. In addition, the breakdown sites of PTFE film are spatially homogeneous when compared to BOPP with considerable clustering as seen in Fig. 7b and d, which presumably due to the lower T_m of BOPP compared to that of PTFE.

Most recently, PTFE films with a thickness below 5 μm have been fabricated by coating the water emulsion of PTFE nanoparticles onto copper foils followed by heat-treatment processes (Fig. 7e-h).[123] Upon thermal annealing, the PTFE particles undergo softening, melting, expanding and leveling in sequence to finally yield a compact film with fiber-like networks. As shown in Fig. 7i, the densely interconnected microstructure affords the 380 °C-treated PTFE film with the highest E_b of 410 MV m^{-1} measured at 25 °C. For the optimized 380 °C-treated PTFE films, high E_b values are obtained with increasing temperature up to 200 °C, *e.g.*, 395 MV m^{-1} and 350 MV m^{-1} at 150 °C and 200 °C, respectively. At an applied field of 350 MV m^{-1} at 200 °C, the PTFE film exhibits a low DC electrical conductivity of 1.4×10^{-10} S m^{-1} and a superior η of 94%. Self-clearing capability has been demonstrated in PTFE film capacitors configured with large-area gold electrodes in 10-mm diameter. Fig. 7j depicts the Weibull plots of the multiple dielectric breakdowns of the optimal PTFE films at 200 °C, in which three repeated tests were conducted at the same site of a PTFE film. Excitingly, the E_b obtained at the second and third times are comparable to the first round, *i.e.*, 346 MV m^{-1} and 361 MV m^{-1} versus 364 MV m^{-1}, signifying that the PTFE films can self-clear well even at elevated temperatures.

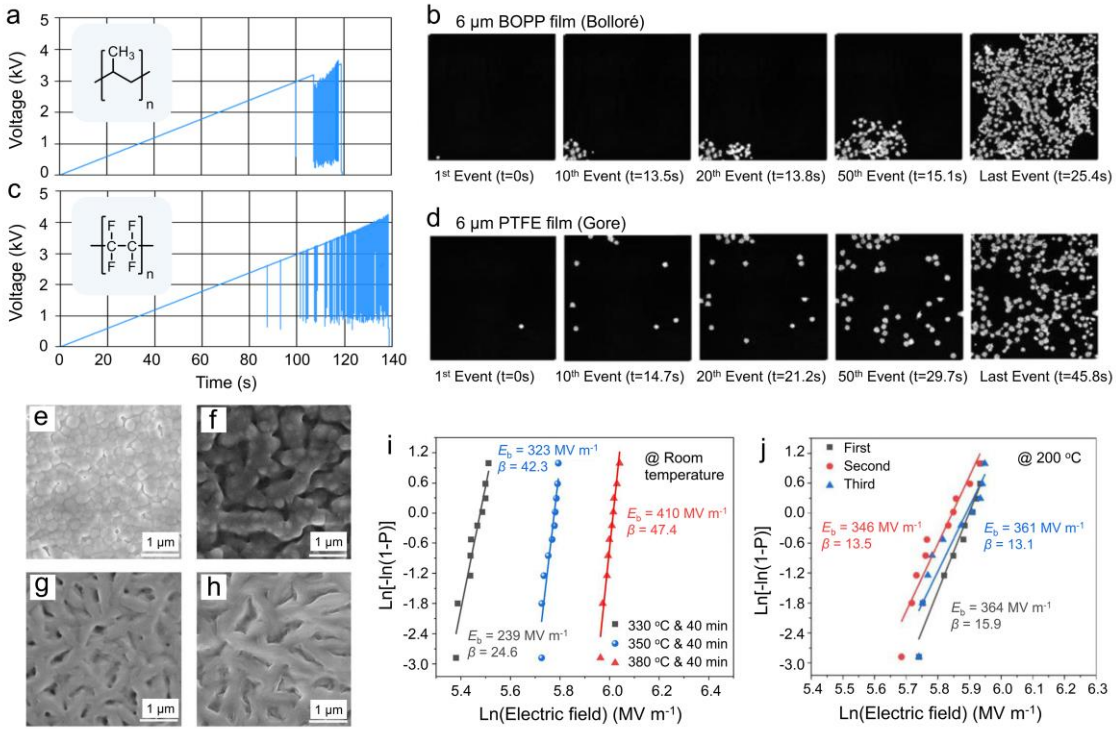

Fig. 7 Voltage ramp showing breakdown events of (a) BOPP and (c) Gore PTFE film. Inset: Chemical structures of PP and PTFE, respectively. Breakdown spatial progression of (b) BOPP and (d) Gore PTFE film.[122] (e) SEM image of the dried PTFE coating on a copper foil before thermal treatment. (f–h) SEM images of the PTFE film treated at 330, 350 and 380 °C, respectively, for 40 min. (i) Weibull distribution of dielectric breakdown strength of the PTFE films prepared at 330, 350 and 380 °C for 40 min, respectively, measured at 25 °C using Au electrodes of 2.5-mm diameter. (j) Weibull distribution of the multiple dielectric breakdown strengths of the PTFE films prepared at 380 °C for 40 min,

measured at 200 °C using Au electrodes of 10-mm diameter.[123] Reproduced from ref. 122 with permission from IEEE and ref. 123 with permission from Elsevier.

While the quality and continuity of the PTFE thin films are remarkably enhanced, the challenges in surface flatness of PTFE films and the adhesion strength and reliability between the electrode and the PTFE films still exist. More recently, Luo *et al.* employed epoxy resin as a coating to smooth the interconnected fiber-liked surface of the PTFE films.[124] It is found that the optimal performance has been achieved for the PTFE film immersed in 0.5 wt% epoxy resin solution, where the local electric field distortion near electrodes was effectively released owing to the improvement of surface flatness. As a result, the PTFE film with an ultrathin epoxy coating delivers the maximum U_e of 1.93 J cm^{-3} at 400 MV m^{-1} and 150 °C with a frequency of 100 Hz, which is 28% greater than that of pristine PTFE films under the same condition.

3.2. Aromatic and heterocyclic dielectric polymers

3.2.1 Aromatic backbone structure with urea groups

The family of polyureas containing urea or thiourea with strong polarities has attracted great attention in the dielectric community.[125] Zhang *et al.* reported thin films of aromatic polyurea (ArPU) prepared via vapor deposition polymerization of 4,4′-diamino-diphenylmethane and 4,4′-diphenylmethanediisocyanate monomers, and aromatic polythiourea (ArPTU) synthesized by polycondensation of 4,4′-diphenylmethanediamine with thiourea.[126,127] The strong dipole moments of urea (~4.56 D) and thiourea (~4.9 D) endow relatively high K values of ~4.2 and ~4.5 at 1 kHz for ArPU and ArPTU, respectively. The ArPU film delivers an E_b of 690 MV m^{-1} and an U_e of 9 J cm^{-3}, whereas the ArPTU film possesses a maximum U_e of 22 J cm^{-3} at a much pronounced electric field of 1 GV m^{-1}. It is hypothesized that the weak coupling among the dipoles due to the separation of thiourea groups by aromatic rings is responsible for low tan δ at low electric fields, whereas the large dipole moments of thiourea moieties act as strong scattering sites to the electrons and ions and may reduce the high-field conduction loss. Improved K values of around ~5.6 and ~6 at 1 kHz are found in the *meta*-aromatic polyurea (*meta*-ArPU) and *meta*-aromatic polythiourea (*meta*-ArPTU) with high volumetric dipole densities.[128,129] It is found that by replacing the two aromatic rings with one ring, the dipole–dipole interaction of polymer backbone is limited, which is favorable to retaining low tan δ. Although numerous polymers consisting of urea functional groups have been developed and shown excellent ambient-temperature dielectric properties as well as fairly invariable K and tan δ over a wide range of temperature up to 200 °C, only poly(arylene ether urea) (PEEU) synthesized from (*m*-phenylenedioxy) dianiline and diphenyl carbonate has been evaluated at elevated temperatures for capacitors.[130] The phenyl ring in the PEEU backbone offers a high T_g of > 250 °C, while the ether linkage boosts the chain flexibility. However, the U_e of PEEU drops by nearly three times from 8.2 J cm^{-3} at 600 MV m^{-1} and room temperature to 2.9 J cm^{-3} at 400 MV m^{-1} and 150 °C. The corresponding η declines from > 95% to < 75% under the same field of 400 MV m^{-1}.

3.2.2 Aromatic backbone structure consisting of ether linkages

A class of aromatic polymers based on the rigid aromatic backbone structure with flexible ether linkages include poly(aryl ether ketone) (PAEK), poly(aryl ether nitrile) (PAEN) and poly(aryl ether sulphone) (PAES),[131–135] in addition to PEEU, has been explored. The most representative one is the PAEK family, which has been extensively used as the insulation component in power electronic modules, nuclear power plant cables, and as the structural support in automotive and aerospace industries due to the excellent thermal and mechanical properties and outstanding radiation, flame and chemical resistances.[136,137] Specifically, all the PAEKs are semicrystalline polymers with T_g varying between 145–155 °C for poly(ether ether ketone) (PEEK) and 155–175 °C for poly(ether ketone ketone) (PEKK), and T_m ranging from 300–345 °C of PEEK to 340–365 °C of PEKK, both of which are determined by the ratio of ketone to ether.[136–138]

The Wang group investigated PEKK film with a K of 3.6 and a tan δ of 0.33% (at 1 kHz and room temperature) that was prepared by melt-pressing the polymer pellets at 360 °C under high pressure.[138] The temperature-dependent dielectric spectra of both K and tan δ were found to be relatively stable with respect to temperature up to 150 °C but exhibit a sudden rise with temperature exceeding 150 °C, which correlates well with the T_g of PEKK (*i.e.*, ~155 °C). This result reveals that the amorphous phases rather than the crystal domains of PEKK play a dominant role in determining the low-field dielectric properties at temperatures higher than T_g. Accordingly, the E_b and U_e also show considerable decreases with the temperature around T_g. For example, the E_b of PEKK decreases from 560 MV m^{-1} at room temperature to 420 MV m^{-1} at 140 °C along with U_e is degraded from 3 J cm^{-3} to 2.37 J cm^{-3}. Poly(phthalazinone ether ketone) (PPEK) with a T_g of about 250 °C was prepared via introducing a rigid asymmetric phenyl phthalazinone unit into the aromatic backbone.[139] As shown in Fig. 8a, PPEK was synthesized by polycondensation of 4-(4-hydroxyphenyl)-2,3-phthalazin-1-one (HPPO) and 4,4′-difluorobenzophenone (DFBP) in dimethylacetamide (DMAc). The phenolate and aza-nitrogen anions, which were formed via deprotonation of HPPO followed by a nucleophilic displacement reaction with activated difluoro monomer DFBP yield PPEK with a high molecular weight. The resulting PPEK exhibits slightly decreased K with respect to PEKK (*i.e.*, 3.5 *vs.* 3.6 at 1 kHz) but an improved invariance in the temperature dependence of K and tan δ spectra, both of which maintain considerably stable with temperature up to 225 °C at 1 kHz, as depicted in Fig. 8b and c. The largely improved T_g is not only responsible for the enhancement in thermal stability of low-field dielectric spectra but also enables the enhanced E_b and capacitive performance at elevated temperatures, *e.g.*, an impressive U_e of 2.1 J cm^{-3} has been achieved at 190 °C with a frequency of 100 Hz. It is worth mentioning that although the E_b of PPEK only decreases slightly from 470 MV m^{-1} at room temperature to 441 MV m^{-1} at 190 °C, the U_e and η actually suffer from monotonic reduction with the increase of electric field and temperature (Fig. 8d and e). The reduction is mainly ascribed to the exponentially growing of conduction current density under high electric fields and especially at elevated temperatures that is dominated by hopping conduction, as shown in Fig. 8f, which has been further verified by fitting AC conductivity within a frequency range between 100 Hz and 1 MHz

(inset of Fig. 8f). These experimental results elucidate again that the electrical conduction plays a decisive role in determining high-temperature high-field electrical properties. Therefore, high T_g and invariable dielectric properties with temperature are not sufficient in order to achieve desirable elevated-temperature capacitive performance.

Recently, another flexible linkage – ether ketone was introduced into the aromatic polyamide (PA) backbone to afford soluble poly(naphthalene ether ketone amide) (PEKNA).[140] This is to address the issue that PAs are notoriously difficult to be processed into high-quality thin films because of their rigid main chain structure and high density of interchain hydrogen bond. Specifically, as shown in Fig. 9a, 1,4-naphthalenediic acid and bis(4-(4-aminophenoxy) phenyl) methanone (BAPPM) were polymerized via Yamazaki phosphorylation reaction to afford PEKNA. Although a T_g of around 250 ℃ was detected in PEKNA, the storage modulus does not decay to zero after undergoing attenuation followed by a phase transition peak at 272 °C, inferring that PEKNA can operate effectively at temperatures higher than its T_g. The peak of X-ray diffraction (XRD) shifts from PEKNA to a smaller angle of the heat-annealed PEKNA (abbreviated as ht-PEKNA) (Fig. 9b). As illustrated in Fig. 9c, the increase in the distance between the molecular chains upon annealing may result in the increased free volume, which in turn improves the dipole flipping ability of ht-PEKNA. It was inferred that the increased active dipole accounts for the enhanced K of ht-PEKNA compared to PEKNA (*i.e.*, 5.3 *vs.* 4.5 at 1 kHz), while the glassy state of the main polymer chain allows maintaining a low tan δ across a wide temperature range, as demonstrated in Fig. 9d. In addition, the annealing process makes the molecular chain more regular and reduces the defect of solution-casted PEKNA, which consequently slims the *D*–*E* loops especially at elevated temperatures (*e.g.*, 200 °C) as compared in Fig. 9e. As a result, a considerably improved U_e of 2.1 J cm^{-3} along with a η of 86.8% were achieved at 400 MV m^{-1} and 200 °C with a frequency of 100 Hz.

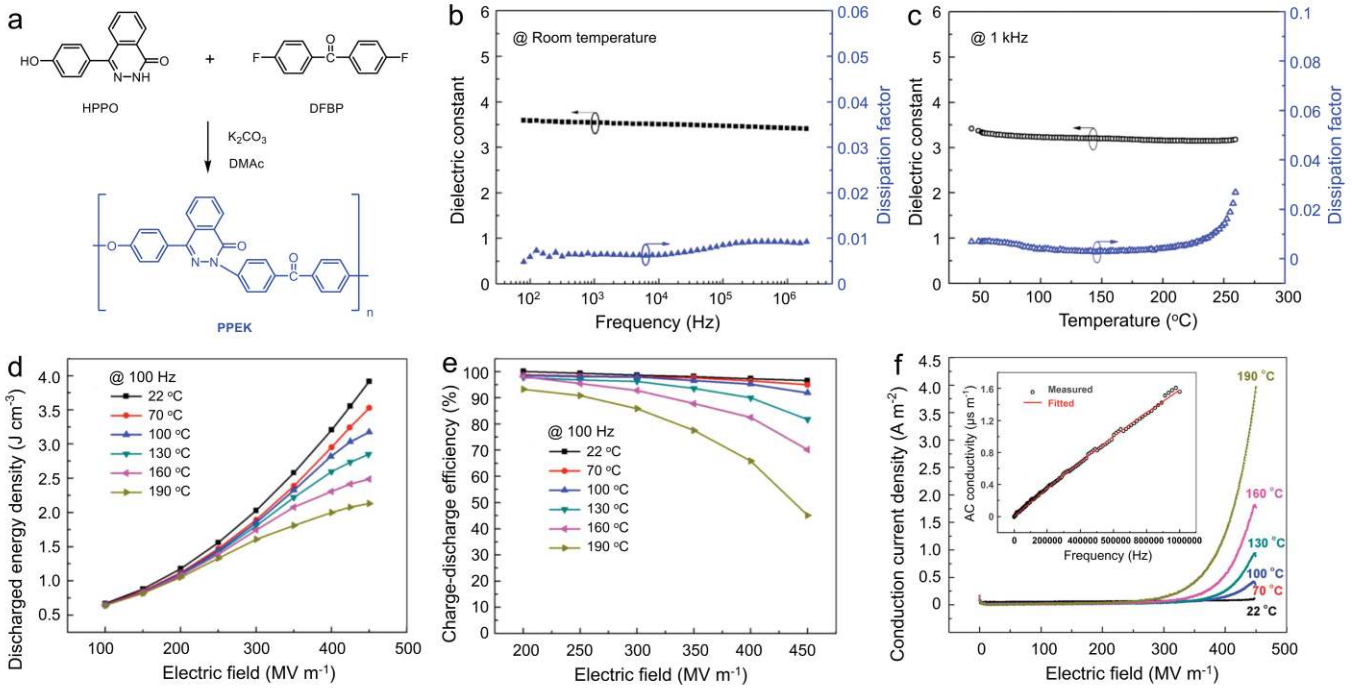

Fig. 8 (a) Synthetic scheme of PPEK. (b) Frequency dependence of the dielectric spectra of PPEK at room temperature. (c) Temperature dependence of the dielectric spectra of PPEK at 1 kHz. (d) Discharged energy density and (e) Charge–discharge efficiency as a function of electric field at varied temperatures. (f) Conduction current density derived from the *D*–*E* loops at varied temperatures. Inset: the measured and theoretically fitted AC conductivity of PPEK.[139] Reproduced from ref. 139 with permission from American Chemical Society.

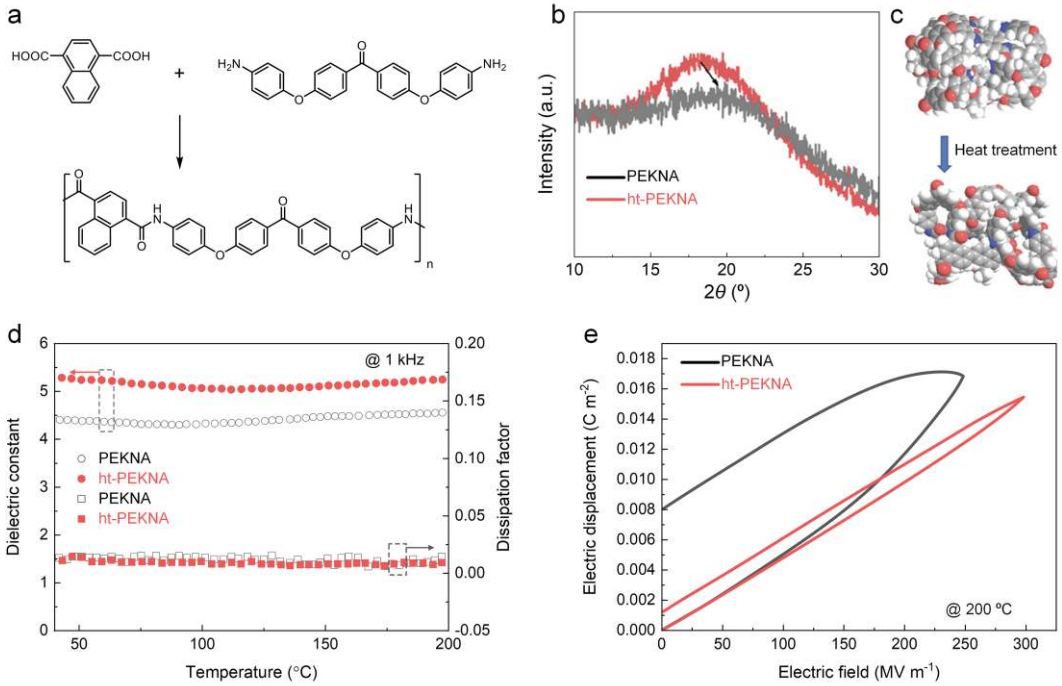

Fig. 9 (a) Synthetic scheme of PEKNA. (b) XRD results of PEKNA and ht-PEKNA. (c) 3D illustration of the PEKNA molecular chain before and after heat treatment. (d) Temperature dependent dielectric spectra of PEKNA and ht-PEKNA at 1 kHz. (e) Unipolar *D*–*E* loops of PEKNA and ht-PEKNA at 200 °C and 100 Hz.[140] Reproduced from ref. 140 with permission from John Wiley and Sons.

3.2.3 Aromatic backbone structure based on imide rings

Another series of the high-temperature aromatic dielectric polymer is based on thermally robust imide rings, in which the most representative is PI. PI is a class of thermoset polymers with amorphous nature, has been known for its exceptional resistance to heat and chemicals, and possesses decent mechanical strength.[141,142] The imide ring structure in the main chain in conjunction with the aromatic backbone endows PIs with exceptional T_g up to 500 ℃. One typical example is Kapton® (Fig. 10a) developed by DuPont in the 1960s, which is prepared from pyromellitic dianhydride (PMDA) and 4,4′-oxydianiline (4,4′-ODA) monomers through a condensation reaction followed by thermal imidization.[143–145] Owing to its high T_g of > 350 ℃, Kapton® has been used extensively as cable insulation in aerospace applications under extreme conditions, *e.g.*, a continuous use temperature ranging from 300–350 °C. Upilex-S® (Fig. 10a) is another commercially available PI from ICI, which is synthesized from monomers of 3,3′,4,4′-biphenyl tetracarboxylic dianhydride (BPDA) and *p*-phenylenediamine (*p*-PDA), with a T_g of around 355 ℃.[146] However, most of these aromatic PIs suffer from the processing challenge in manufacturing thin films with thickness < 10 μm because of their high degrees of aromaticity. Polyamideimide (PAI) is another typical imide-based heat resistance amorphous aromatic polymer, which was developed to improve the processability of PI by introducing amide moieties (Fig. 10a).[147–149] A commercial representative is Torlon® grade PAI from Solvay, exhibiting a T_g of 275 ℃. Similar to PIs, PAIs resist most chemicals and can operate in harsh thermal and chemical environments even under severe stress and show little to no creep, wear, and chemical degradation.[147] Compared to commercially available PIs (*e.g.*, Kapton®), PAIs typically exhibit a lower endurance of long-term service temperature but a higher fracture toughness. In terms of electrical applications, PAIs have long been used as insulation materials for copper wires and the outer painting of enameled wires.[148,149] Additionally, as PAIs display good processability and dissolvability, they can be readily solution-processed into thin polymer capacitor films. Other flexible moieties such as ether linkage and alkyl group have also been introduced into the aromatic backbone to improve the processability of PIs. One example is PEI (Fig. 10a),[60] trademarked as Ultem® by SABIC, which is synthesized from the disodium salt of bisphenol A and 1,3-bis(4-nitrophthalimido) benzene. The presence of flexible linkages endows the thermoplastic nature of PEI, which substantially enhances their processability, including extrudable, injection- and compression-moldable, and soluble in various organic solvents such as *N*-Methyl-2-pyrrolidone (NMP).[150] In addition to the structural and electrical insulation applications under extreme conditions such as automotive and aerospace,[151,152] 5-μm thin PEI films processed by melt-extrusion followed with mechanical stretching are employed as dielectric films in DC-DC converters.[25,60] While the increase in flexibility offered by the ether linkages and alkyl groups of PEIs is achieved at the expense of a largely reduced T_g (*e.g.*, ~217 °C for Ultem® PEI), which is considerably lower than many of the richly aromatic PIs, the incorporated groups break the long-range conjugated structure of PIs. It is believed that the weakening of bond conjugation would impede electron delocalization, which results in a wider bandgap and in turn favors concurrent increases in electrical resistivity and breakdown

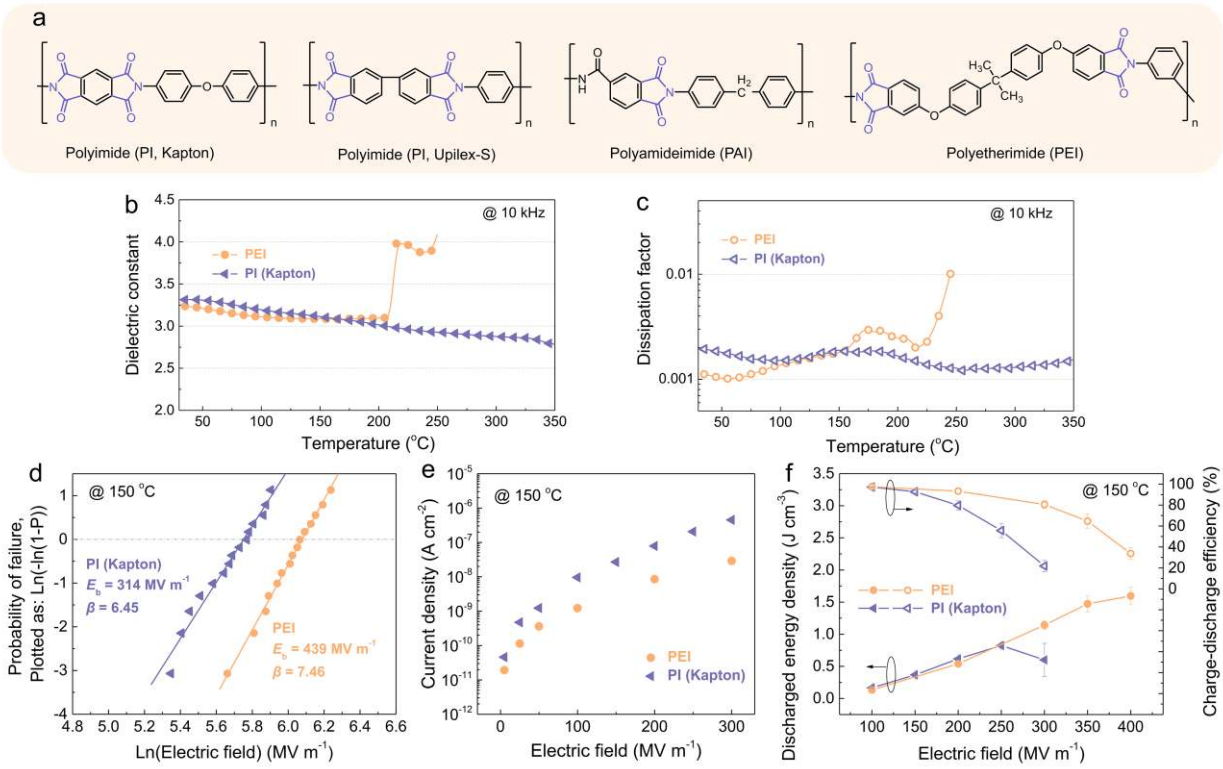

Fig. 10 (a) Chemical structures of Kapton® PI, Upilex-S® PI, PAI and PEI. Temperature-dependent (b) dielectric constant and (c) dissipation factor of Kapton® PI and PEI measured at 10 kHz, respectively.[6] (d) Weibull distribution of breakdown strength and (e) leakage current as a function of electric field of Kapton® PI and PEI at 150 °C, respectively. (f) Discharged energy density and charge–discharge efficiency of Kapton® PI and PEI as a function of electric field at 150 °C.[67] Reproduced from ref. 6 with permission from Springer Nature and from ref. 67 with permission from John Wiley and Sons.

strength of dielectric polymers. The bandgaps of Kapton® PI and Ultem® PEI calculated by density functional theory (DFT) are ~2.6 eV and ~3.2 eV, respectively.[153] However, it should be noted that, compared to inorganic crystals, the presence of amorphous domains and amorphous-crystalline interfaces in (semi)crystalline polymers significantly complicates the modeling of polymers. Regarding the prediction of the electronic structure of polymers, numerous factors, *e.g.*, polymer chain configuration and the interaction between polymer chains, critically affect the electronic structures of polymers.

The temperature dependence of K and tan δ, dielectric breakdown, electrical conduction and capacitive energy storage properties of Kapton® PI and Ultem® PEI are compared in Fig. 10b-f.[6,61,67] As shown in Fig. 10b and c, Kapton® PI exhibits a steadily decreased K from 3.3 to 2.8, and a well-retained low tan δ (*e.g.*, < 0.3%) with temperature rising from 25 ℃ to 350 ℃. In sharp contrast, although Ultem® PEI retains much stable K ranging between 3.1 and 3.2 from 25 ℃ to 200 ℃, its relatively low T_g results in sudden changes in both K and tan δ spectra of PEI with temperature up to 200 ℃. An apparent relaxation peak is also seen in the tan δ spectrum around 175 ℃. Unexpectedly, the high-temperature dielectric properties of PEI, especially under high electric fields, are not compromised with a remarkably decreased T_g with respect to PI. For example, PEI delivers both higher E_b and β of 439 MV m^{-1} and 7.46 when compared to 314 MV m^{-1} and 6.45 of PI, respectively, at 150 ℃ (Fig. 10d). The larger β value derived from Weibull statistics stands for a narrower data dispersion. Additionally, the leakage current densities of PEI are also smaller than those of PI at 150 °C, *e.g.*, 2.89×10^{-8} A cm^{-2} versus 4.51×10^{-7} A cm^{-2} under an applied field of 300 MV m^{-1} (Fig. 10e). The larger E_b along with the smaller leakage current are believed to be attributed to a wider bandgap of PEI, which leads to the much better capacitive properties of PEI than PI (Fig. 10f). For instance, under an electric field of 300 MV m^{-1} and at 150 °C, the η of PI is only 21.8% whereas PEI still retains a high η of 80.5%, resulting in the U_e of PEI about twice that of PI (*i.e.*, 1.14 J cm^{-3} *vs.* 0.59 J cm^{-3}). While both PI and PEI show a typical decrease in capacitive performance with the further increase of temperature, PEI remains fairly efficient in delivering a η of ~60% at 250 MV m^{-1} and 200 °C, a temperature very close to its T_g. On the contrary, the η of PI is almost reduced to zero under the same condition, signifying that the maximum use temperature of PI at high fields is much below its T_g. In addition, note that a loss of U_e by 5% is typically defined as the failure of capacitors in pulsed power applications.[154] While no breakdowns have been detected in both Kapton® PI and Ultem® PEI during charging–discharging cycles at 150 °C and 200 MV m^{-1}, considerable variations in U_e (*i.e.*, ~8.9% for Kapton® PI within 30 000 cycles and ~6.2% for Ultem® PEI within 55 000 cycles) manifest that a further enhancement of high-temperature cyclic reliability of these imide ring-based polymers is highly demanded.[61,155]

Another major challenge of the imide-linked aromatic polymers in film capacitors may arise from high moisture sensitivity and high water uptake owing to the imide ring structure in the aromatic

backbone. This issue could be addressed by impregnating the windings with insulating fluid and by hermetically sealing the interior.[47] In addition, the considerably poor self-clearing capability in the aromatic backbone structures with respect to BOPP calls for intensive research in structural optimization. Another limitation of PEIs is the unavoidable presence of solvent and the formation of water or carbon dioxide during the condensation reaction. Both the condensation side-products and the solvents need to be fully removed prior to the processing of polymer in order to achieve high electrical insulation properties and low loss.[60] Similarly, the requirement of a post-curing procedure at above its T_g in PAIs complicates the thin film processing.[156]

3.2.4 Beyond high T_g: electronic structure consideration

Fig. 11a shows the polymers based on the aromatic backbone with exceptional high T_g or high thermal resistance. FPEs were originally developed by 3M in the 1980s, representing a class of amorphous polyarylates synthesized from the monomers of fluorene bisphenol and phthalic chlorides. Although a considerably high T_g (*i.e.*, ~330 ℃) of FPE enables the relatively stable K across a wide range of temperature (*e.g.*, ~3.5 at 25 °C with < 5% reduction at 300 °C, at 1 kHz), similar to PIs, the exponentially increased conduction loss leads to undesirable capacitive properties at elevated temperatures. For example, at 150 ℃, which is much lower than its T_g, the U_e of FPE is ~1.2 J cm^{-3}, which is twice as high as that of Kapton® PI but a quarter smaller than that of PEI.[6] Up to now, small-scale metalized film capacitors based on FPE have been produced with the aim to be a commercial substitute for BOPP.[157] It was found that the diamond-like hydrocarbon linkage in FPE modified with 4,9-diamantyl moiety significantly enhances the T_g to 450 ℃ and yields stable K and tan δ values (*e.g.*, 3.5 and < 0.4%, at 10 kHz) between 25 ℃ and 350 ℃.[158]

Rigid-rod polymers, known for their outstanding thermal-mechanical stability due to rod-like extended backbone in conjunction with the *para*-linked aromatic/heterocyclic rings, are often used as high-temperature high-strength fibers.[159–161] It was found that polybenzobisthiazole (PBT) and polybenzoxazole (PBO) exhibit the K values of 2.9 and 2.8, respectively, at 1 kHz with variations < 10% across the temperature range from 25 °C to 300 °C.[162] However, the tan δ of both polymers increases by nearly an order of magnitude with increasing temperature from room temperature to 250 °C at 10 kHz, which may account for the fact that this series of rigid-rod aromatic polymers remain unexplored as film capacitor dielectrics so far.

Polybenzimidazoles (PBIs) are another class of aromatic polymer with ultra-high T_g.[163,164] The most typical one is poly(2,2′-*m*-phenylene-5,5′-bibenzimidazole) (*m*-PBI) exhibiting a high T_g of around 430 °C, which is prepared through the condensation of monomers of tetraaminobiphenyl and either diphenyl-isophthalate or isophthalic acid, and has been commercialized by Celanese in the 1980s. The K and tan δ of PBI are about 3.5 and ~2% at 60 Hz and 20 °C, but increases dramatically to 11 and ~50% at 300 °C.[165] Similar to the imide ring, the imidazole moiety with strong polarity in the aromatic backbone results in the unfavorable moisture sensitivity of PBI, which can cause the aging of dielectrics and increase the difficulty of the device packaging. Although capacitive properties of PBI haven't been examined to date, it is argued that the resulting high T_g is achieved at the expense of bandgap which may account for the unfavorable tan δ values and the considerable variations in both K and tan δ with increasing temperature. Specifically, the presence of the imidazole ring affords a highly conjugated backbone structure of PBI, which reduces the energy barrier for charge transport and consequently deteriorates breakdown strength and induces pronounced leakage current under high temperatures and high fields.

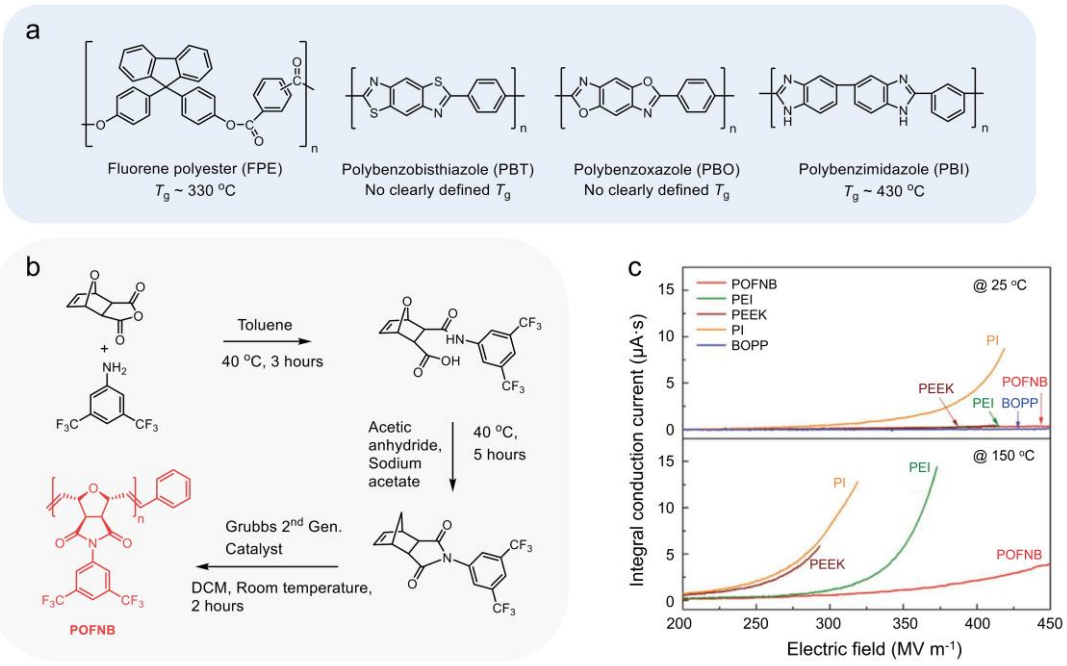

Fig. 11 (a) Chemical structures of FPE, PBT, PBO and PBI. (b) Synthetic scheme of POFNB. (c) Comparison of integral conduction current among POFNB, PEI, PEEK, PI and BOPP.[153] Reproduced from ref. 153 with permission from John Wiley and Sons.

In addition to T_g, it is recognized that the electronic structure of dielectric polymers plays a vital role in determining high-temperature high-field capacitive performance. Recently, DFT computations reveal a typical inverse correlation between the T_g values and bandgaps in high-temperature aromatic polymers including PI, PAI, PEI, PEEK, PEN and PET.[153] This result indicates that, although the T_g values found in the aromatic polymers are highly desirable, the reduced bandgaps owing to high degrees of aromaticity in the aromatic polymers may significantly compromise their utilization as capacitive materials under high applied fields and elevated temperatures. Polyoxafluoronorbornene (POFNB) with a saturated fused bicyclic structure in the backbone was synthesized through a ring-opening metathesis polymerization of oxafluoronorbornene monomer using Grubbs 2nd generation catalyst (Fig. 11b).[153] POFNB has a T_g of 186 ℃ and a relatively low K of about 2.5 across the temperature range of 20–180 ℃ at 1 kHz. Interestingly, the nonplanar structure and non-conjugated polymer backbones of POFNB yield a wide bandgap of 4.9 eV, exceeding the current polymers with similar T_g values. Consequently, POFNB efficiently suppresses conduction current at high applied fields up to 150 ℃, outperforming other dielectric aromatic polymers as compared in Fig. 11c.

To summarize, the aliphatic dielectric fluoropolymers represented by PTFE show outstanding thermal stability along with ultralow tan δ and high E_b values. Their relatively low K needs to be addressed in order to achieve high energy densities in PTFE-based film capacitors. On the other hand, the aromatic and heterocyclic dielectric polymers consisting of urea groups, ether linkages and imide rings typically possess higher K and greater T_g values than PTFE, it remains challenging to design new aromatic and heterocyclic structures of dielectric polymers exhibiting low dielectric loss at high fields and elevated temperatures. It is desirable to disrupt conjugated electronic structure, while retaining large K and high T_g values, and increase the ratio of (oxygen + hydrogen) to carbon for improved self-clearing capability.

4. Dipolar grafting approach to high-temperature dielectric polymers

The sharply increased conduction loss with applied electric fields has been attributed in part to large-scale molecular motions of polymer backbones. To address this issue, dipolar glass polymers have been proposed, in which the chain motion is largely frozen to confine dielectric/conduction loss. Meanwhile, polar groups of dipolar glass polymers can only rotate locally to enhance orientational polarization and the K value.[166] Note that the aforementioned high-T_g dielectric polymers with aromatic and heterocyclic backbone structures have limited K values *i.e.,* ≤ 4 at 1 kHz. In recent decades, dielectric polymers consisting of different polar groups have been developed based on both nonpolar and polar polymeric backbones, which can be divided into main-chain and side-chain dipolar grafting polymers depending on the location of dipolar moieties.[43] Typical polar units include hydroxyl (–OH), carbonyl (–C(=O)–), nitro (–NO_2), cyano (–CN), sulfonyl (–SO_2–), and thiourea (–NHC(=S)NH–) functional groups with incremental dipole moment from ~1.7 D, ~2.3 D, ~3.6 D, ~3.8 D, ~4.3 D to ~4.9 D, respectively.

4.1. Dipolar grafting on main chain of polar dielectric polymers

Examples of the main-chain dipolar grafting polymers include but are not limited to aromatic PIs,[167–169] PAs,[170] and ArPUs.[171–173] The dielectric properties of the main-chain dipolar grafting polymers can be modulated by using different polar chain segments in the polymer backbone, incorporating additional permanent dipoles, varying conjugation length and controlling the degree of crystallinity.[44,174] For instance, the K values of ArPTUs are readily tuned through grafting polar chains with different lengths and flexibilities.[171–173] However, the energy storage performance of the main-chain-modified ArPUs and ArPTUs at high temperatures is rarely investigated.

The PI-based dielectric polymers have been ideal platforms for readily tuning backbone structure by selecting different combinations of dianhydride and diamine monomers. To date, numerous studies have focused on the development of the correlation between multi-physical properties (*e.g.*, T_g values and frequency dependence of K and tan δ) and the molecular structure of PIs.[167–169,175–180] By introducing a –$C(CF_3)_2$– bridge into the dianhydride monomer, the resulting fluorinated PIs show a monotonic reduction in the K value with increasing fluorine content, *e.g.*, a K of 2.4 at 100 °C and 100 Hz with 30.7 wt% fluorine.[175] It is found that the bulky –$C(CF_3)_2$– repeating units in the main backbone reduce chain mobility and dipole density, which consequently decreases the K values of the PIs. In contrast, by introducing a series of polar moieties with high dipole moments, including bipyridine, bipyrimidine and crown ether groups, into the aromatic backbone of PIs, high K values ranging from 5.9–7.2 at 1 kHz that are stable from 275–343 °C are obtained.[176–178]

While a large number of studies have confirmed that incorporating functional groups with large dipole moments into the main chain of PIs can effectively increase the K and U_e values, the polar groups or long flexible segments typically introduce additional dielectric/conduction loss and deteriorate breakdown strength.[181] The current studies of PIs mainly center on the dielectric properties and capacitive performance at ambient temperature and temperature-dependent dielectric spectroscopy, while the high-temperature capacitive performance of the dipolar-grafted PIs has not been extensively investigated. A systematic study has been conducted regarding the relationship between the monomer structures and dielectric properties of the cyano-containing PIs (PI-CNs), including high-field D–E loops at elevated temperatures.[170–172] A series of PIs with a single cyano group per repeating unit were synthesized through a condensation reaction followed by thermal imidization between a diamine, such as the asymmetric 2-(3-aminophenoxy)-6-(4-aminophenoxy) benzonitrile (3,4-APBN), symmetric 2,6-bis(3-aminophenoxy) benzonitrile (3,3-APBN) and symmetric 2,6-bis(4-aminophenoxy) benzonitrile (4,4-APBN), and a dianhydride, such as 1,1,1,3,3,3-hexafluoropropane dianhydride (6FDA), 4,4′-oxydiphthalic dianhydride (OPDA), 4,4′-benzophenonetetracarboxylic dianhydride (BTDA), PMDA and 3,3′,4,4′-diphenylsulfone tetracarboxylic dianhydride (DSDA) (Fig. 12).[170,171] It was found that the presence of the cyano group improves the K from 2.92 of the analogous PI without cyano groups to 3.1–3.5 at room temperature and 1 kHz. In addition, the asymmetric structure of the aromatic diamine monomer can improve the processability and enhance K values of PIs. In the following work, PIs with even larger dipole moments were developed based on the polymerization of the aromatic diamine containing three cyano groups in each repeating unit with dianhydrides (Fig. 12), which yields

the highest K of 3.75 at room temperature and 1 kHz.[172] The dipole moment of the dianhydride also plays an important role in determining K of the cyano-containing PIs, where the degree of enhancement in K gradually decreases in the order of PMDA > OPDA > 6FDA > BTDA for PIs employing different dianhydrides. Additionally, it was found that the *para–para* linkage in the diamine yields a larger K than the *meta–para* and *meta–meta* linkages between dianhydride and diamine moieties, which is attributed to easier dipole rotation around the *para–para* bonds. At 190 ℃ and 10 Hz, the dipolar grafting PI based on a condensation of PMDA dianhydride and the diamine with three cyano groups and a *para–para* linkage exhibits an U_e of ~0.22 J cm^{-3} and a conduction loss of < 30% under an applied electric field of 100 MV m^{-1}.[171] The strategy of using cyano groups to enhance K is also applicable to non-aromatic polymers. An example is poly(acrylonitrile-*co*-butadiene-*co*-styrene) (ABS) (Fig. 13b), which shows a high K of 4.6 at room temperature and 1 kHz that is stable up to T_g (*i.e.*, 128 °C).[182] Interestingly, ABS exhibits an excellent high-field performance even near its T_g, which is rarely seen in amorphous dielectric polymers. As shown in Fig. 13a, the E_b and β of ABS decline modestly from 505 MV m^{-1} and 26 to 480 MV m^{-1} and 24, respectively, as temperature increases from room temperature to 120 °C. The slim *D–E* loops measured at 120 °C are suggestive of small energy loss

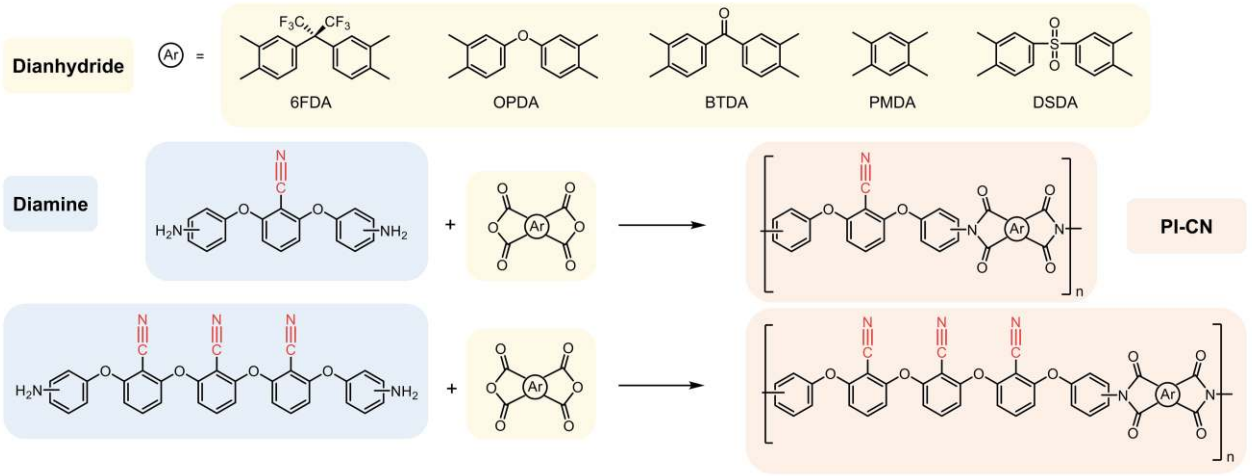

Fig. 12 Synthetic scheme of cyano-containing polyimides (PI-CNs), and chemical structures of dianhydride monomers of 6FDA, OPDA, BTDA, PMDA, DSDA and diamine monomers bearing one and three cyano groups.[171] Reproduced from ref. 171 with permission from The Royal Society of Chemistry.

during charging–discharging cycles (Fig. 13b). The U_e and η at 120 ℃ are only slightly inferior to its room-temperature performance, *e.g.*, 6.7 J cm^{-3} and 75% at 500 MV m^{-1} versus 7.3 J cm^{-3} and 80% at 525 MV m^{-1} (Fig. 13c). In addition, the cycling tests up to 10 0000 times indicate the excellent reliability of ABS with variations smaller than 3% at both room temperature and 90 ℃.

4.2. Dipolar grafting on side chain of polar dielectric polymers

The mobility of dipolar moieties grafted onto the polymer backbone is rather limited due to the rigidity of the aromatic or heterocyclic backbone. To utilize the orientational polarization for further improvement of the K value of dipolar grafting polymers, the polar groups have also been introduced into dielectric polymers by attaching to the side chains.[44]

Representative examples are the PC- and PEI-based polymers with cyano groups grafted on their side chains.[25,183] By attaching cyanomethyl (–CH_2CN) dipole onto the side chain of a bisphenol A-typed PC to yield CN-PC, a K at 1 kHz and 25 ℃ is enhanced to 4 for CN-PC compared to 2.9 for the unmodified PC, while tan δ keeps as low as 0.5%. However, both K and tan δ of PC-CN suffer from strong temperature dependence when temperature exceeds 125 °C, which is presumably attributed to large ionic conduction from impurities.[25] The Zhu group developed a series of dipolar glassy polymers containing side-chain grafted sulfonyl groups.[184–186] For instance, poly[2-(methylsulfonyl)ethyl methacrylate] (PMSEMA) with a high K of ~11 (at 25 °C and 10 Hz) was synthesized by grafting a methylsulfonyl unit through a flexible ether group.[184] The K value is nearly three times larger than that of the control polymer, *i.e.*, polymethyl methacrylate (PMMA). Sulfonylated polyepichlorohydrin (PECH) and poly[3,3-bis(chloromethyl)oxetane] (PBCMO) bearing one and two methylsulfonyl groups per repeating unit, respectively, also exhibit significantly enhanced K relative to the unmodified polymers.[184] It was found that the dipolar grafting using two sulfonyl groups affords higher K, which is unfortunately accompanied by larger tan δ in comparison to the monosulfonylated grafting approach. Moreover, the sulfonyl grafted aliphatic polymers have relatively low T_g (< 125 °C), which limits their use at elevated temperatures.

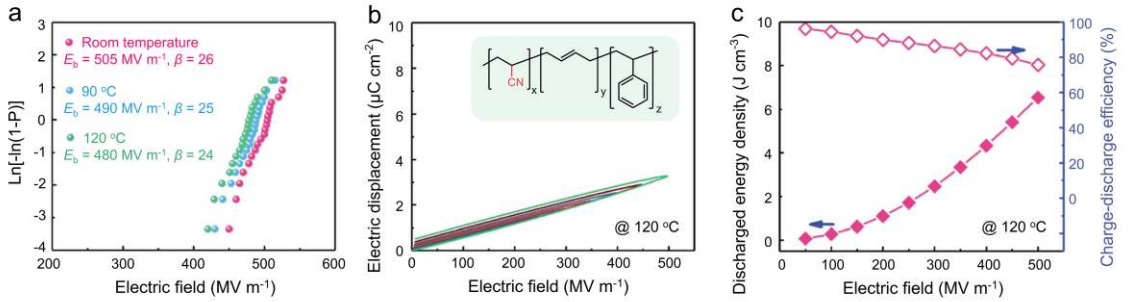

Fig. 13 (a) The Weibull distribution of dielectric breakdown strength at room temperature, 90 °C and 120 °C for ABS, (b) Unipolar *D*–*E* loops of ABS under varied electric fields at 120 °C. Inset: the chemical structure of ABS. (c) Discharged energy density and charge−discharge efficiency of ABS as a function of electric field at 120 °C.[182] Reproduced from ref. 182 with permission from The Royal Society of Chemistry.

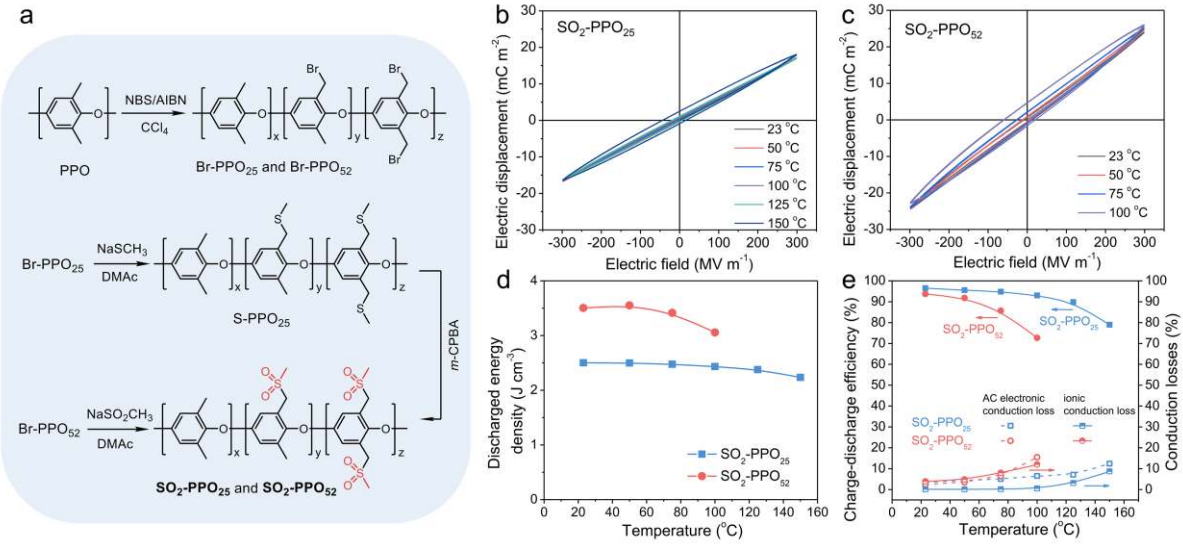

Fig. 14 (a) Synthetic scheme of the sulfonylated PPOs (SO_2-PPO_{25} and SO_2-PPO_{52}). Bipolar *D*–*E* loops at varied temperatures of (b) SO_2-PPO_{25} and (c) SO_2-PPO_{52}. (d) Discharged energy density and (e) Charge–discharge efficiency as a function of temperature of SO_2-PPO_{25} and SO_2-PPO_{52}, respectively, measured at 300 MV m^{-1} with a frequency of 1 kHz.[187] Reproduced from ref. 187 with permission from John Wiley and Sons.

To enhance the heat tolerance of dipolar glass polymers, poly(2,6-dimethyl-1,4-phenylene oxide) (PPO) was selected because of its high T_g of ~220 ℃. Fig. 14a depicts the synthesis of sulfonylated PPO (SO_2-PPO) with different dipole grafting densities were synthesized via post-functionalization.[187] First, bromine was anchored onto the side chain of PPO using bromosuccinimide/azobis(isobutyronitrile) (NBS/AIBN) in CCl_4 to afford Br-PPO_{25} and Br-PPO_{52}, where the subscripted numbers represent the degree of bromination. Then, SO_2-PPO_{25} was prepared by nucleophilic substitution of Br-PPO_{25} with $NaSCH_3$ to yield S-PPO_{25} followed by oxidization of the sulfide with *meta*-chloroperoxybenzoic acid (*m*-CPBA). Owing to the direct conversion and easy access to $NaSO_2CH_3$, the nucleophilic substitution of Br-PPO_{52} with $NaSO_2CH_3$ is a more preferred route for the synthesis of SO_2-PPO dipolar grafting polymers. The resulting SO_2-PPO_{25} and SO_2-PPO_{52} retain the amorphous nature of PPO with comparable T_g values of 211 ℃ and 228 ℃, respectively. The highly rigid backbone of SO_2-PPO would provide sufficient free volume for dipole rotation of methylsulfonyl groups below their T_g, which enhances the orientational polarization and gives rise to the *K* values of 5.9 and 8.2 at room temperature at 1 kHz for SO_2-PPO_{25} and SO_2-PPO_{52}, respectively, along with low tan δ values (*e.g.*, 0.3% for SO_2-PPO_{25} at 100 °C and 1 kHz). High U_e values of 22 J cm^{-3} for SO_2-PPO_{25} and 24 J cm^{-3} for SO_2-PPO_{52} were obtained at room temperature with a frequency of 1 kHz. However, as the applied electric field increases, the conduction loss increases concurrently, resulting in the reduction of η, *e.g.*, > 95% at 100 MV m^{-1} *vs.* < 75% at 800 MV m^{-1} of SO_2-PPO_{52} at room temperature. It is noteworthy that the typical tradeoff between *K* value and energy loss becomes more intricate with the increase of temperature and electric field. Fig. 14b and c show the bipolar *D*–*E* loops for SO_2-PPO_{25} and SO_2-PPO_{52} under an applying field of 300 MV m^{-1} at different temperatures. Slim loops are retained until 125 °C for SO_2-PPO_{25}, whereas SO_2-PPO_{52} displays much broad loops when temperature reaches 100 °C. Moreover, as compared in Fig. 14d, while SO_2-PPO_{25} with a lower *K* delivers a lower U_e than SO_2-PPO_{52}, the decrease in U_e of SO_2-PPO_{25} at elevated temperatures is much less significant compared to that of SO_2-PPO_{52}. The decrease in U_e originates from the increased energy loss due to electronic conduction as the major

loss component and ionic conduction as the minor contributor, as shown in Fig. 14e. Unlike SO_2-PPO_{25} with a lower dipole grafting density, SO_2-PPO_{52} presents significant AC conduction as temperature is above 75 ℃, which is postulated that the presence of more sulfonyl dipoles in SO_2-PPO_{52} that favors charge injection from the metal electrodes at elevated temperatures.

More recently, a concept of friction-free dipolar glass polymers was demonstrated on the polymers of intrinsic microporosity (PIM).[188] Similar to SO_2-PPO, polar sulfonyl groups were attached to the side chain of an organosoluble PIM to yield sulfonylated PIM (SO_2-PIM), whose chemical structure is illustrated in the inset of Fig. 15a.[189] The nano-sized pores were verified by wide-angle X-ray diffraction (WAXD) and transmission electron microscopy (TEM), as seen in Fig. 15a and b. The nanopores in PIMs provide large free volume for friction-free rotation of sulfonyl dipoles on side chain before glass transition (*i.e.*, above the thermal degradation temperature of ≥ 350 ℃), which is helpful to maintain low tan δ. The grafted sulfonyl groups are able to promote orientational polarization and in turn enhance the K. Consequently, SO_2-PIM displays a tan δ as low as 0.5% along with a high K of 5.3 at 40 °C and 1 kHz and an U_e of 17 J cm^{-3} with a high η ≥ 90% at 770 MV m^{-1}. More impressively, as shown in Fig. 15c, slim loops of PIMs, *i.e.*, high η values of 94% and 88% were realized at 175 °C and 200 °C, respectively, under 200 MV m^{-1}.

The dipolar grafting strategy to high-temperature dielectric polymers has witnessed gratifying progress especially in tailoring K value via the use of functional groups with different dipole moments on main or/and side polymer chains. Special attention shall be placed on resolving the paradox between K values and energy losses (*i.e.*, tan δ at low field and conduction loss at high field) for thus-designed polymers. In addition to dipole moment of the grafted segments, the chain length and mobility as well as grafting density also play key roles in determining high-temperature capacitive performance, which demands a comprehensive consideration.

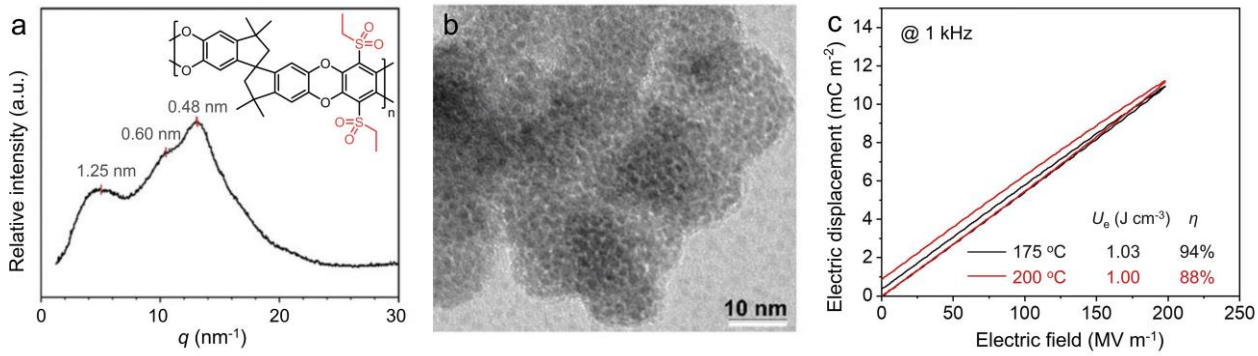

Fig. 15 (a) One-dimensional WAXD profile of SO_2-PIM. The multiple broad peaks correspond to different pore sizes ranging from 0.5–1.25 nm (the chemical structure of SO_2-PIM is in the inset). (b) Bright-field TEM image of SO_2-PIM stained by RuO_4 for 10 min, the polymer struts appear dark and the pores appear brighter, the average pore width was *ca.* 0.6 nm with a run length of 1.2–1.5 nm. (c) Unipolar *D*–*E* loops of SO_2-PIM at 175 °C and 200 °C, respectively, under 200 MV m^{-1} with a frequency of 1 kHz.[189] Reproduced from ref. 189 with permission from The Royal Society of Chemistry.

5. Crosslinking strategy toward high-temperature dielectric polymers

5.1. Thermoset dielectric resins

Epoxy resins are one of the most representative thermoset resins that are extensively used as the main insulation component for high-voltage power equipment.[190,191] However, it has been challenging to process epoxy resin into free-standing thin films due to the poor ductility and large residue stress of the cured product.[192,193] Recently, a crosslinked epoxy resin network consisting of asymmetric alicyclic amine-polyether amine molecular chain structures was prepared via the Mannich reaction.[104] As shown in Fig. 16a, 12 μm-thick films were fabricated by inserting epoxy resin-hardener mixtures between two pieces of PET release films followed by hot-pressing and thermal curing. The optimized performance was obtained by tailoring the asymmetric structure with a mole ratio of 1:1.6 of alicyclic amine and polyether amine components. Different from the grafting approach, the asymmetric design for hardeners can facilitate the chain realignment under an applied field, which introduces additional dipole moments and consequently leads to a relatively high K of 4.4–4.6 at 1 kHz and room temperature. The rigid rings in the alicyclic amine chain yield a T_g of around 136 °C, whereas the polyether amine moieties with rotatable ether linkages are responsible for its mechanical flexibility, which afford the epoxy films fairly desired cyclic capability (*e.g.*, 3.89% decrease over 20 000 charging–discharging cycles at 120 °C and 200 MV m^{-1}). With an E_b of > 600 MV m^{-1}, an U_e up to 9.12 J cm^{-3} along with a η of 90% was obtained at 550 MV m^{-1}, the values are comparable to the best values achieved for linear polymers at room temperature. However, U_e decreases monotonically from 4.5 J cm^{-3} at 70 °C to 3 J cm^{-3} and 1 J cm^{-3} at 100 °C and 120 °C, respectively, with their η values > 90%. Impressively, the low element ratio of carbon to (hydrogen plus oxygen) in the crosslinked molecular structure offers the self-clearing ability of the metalized epoxy film. As revealed by scanning electron microscopy (SEM) and energy dispersive spectroscopy (EDS) element mapping, an electro-devaporization area can be clearly observed on the surface of epoxy films after breakdown occurs (Fig. 16c and d), in which the carbonization area of the hole is isolated with no detectable Au element. As shown in Fig. 16e, no noticeable degradation was found in the comparison of the *D*–*E* loops before

and after breakdown, further verifying the success of self-clearing. After an initial breakdown at 510 MV m^{-1}, the self-cleared epoxy film can achieve 90% U_e of the first cycle.

Divinyltetramethyldisiloxane-bis(benzocyclobutene) (BCB) monomer can be crosslinked by thermal- or photo-assisted approaches, *e.g.* the [4+2] Diels–Alder reaction between the alkene unit and the *o*-quinodimethane intermediate from ring-opening of the benzocyclobutene, to yield crosslinked BCB (*c*-BCB), as shown in Fig. 17a.[194] While *c*-BCB undergoes no glass transition before thermally decomposition at > 350 ℃, it displays a remarkably stable *K* and low tan δ (< 0.2%) in the frequency range between 100 Hz and 1 MHz at 150 ℃ and over a wide temperature range from 25 ℃ to 300 °C (Fig. 17b and c).[6,67] As expected, the thermally- and electrically-activated charge carriers increase exponentially with temperature and applied electric field, leading to sharply increased conductivities and high conduction losses. For example, the electrical conductivity increases from 2.5×10^{-16} S m^{-1} at 25 °C to 6.1×10^{-12} S m^{-1} at 250 °C under an applied field of 50 MV m^{-1}. It was found that the addition of inorganic nanofillers with large bandgaps, such as boron nitride nanosheets (BNNSs) with a bandgap of ~6 eV and Al_2O_3 nanoplates with a bandgap around 9 eV, can effectively enhance both U_e and η by reducing the leakage current at high electric fields and elevated temperatures (Fig. 17).[6,67]

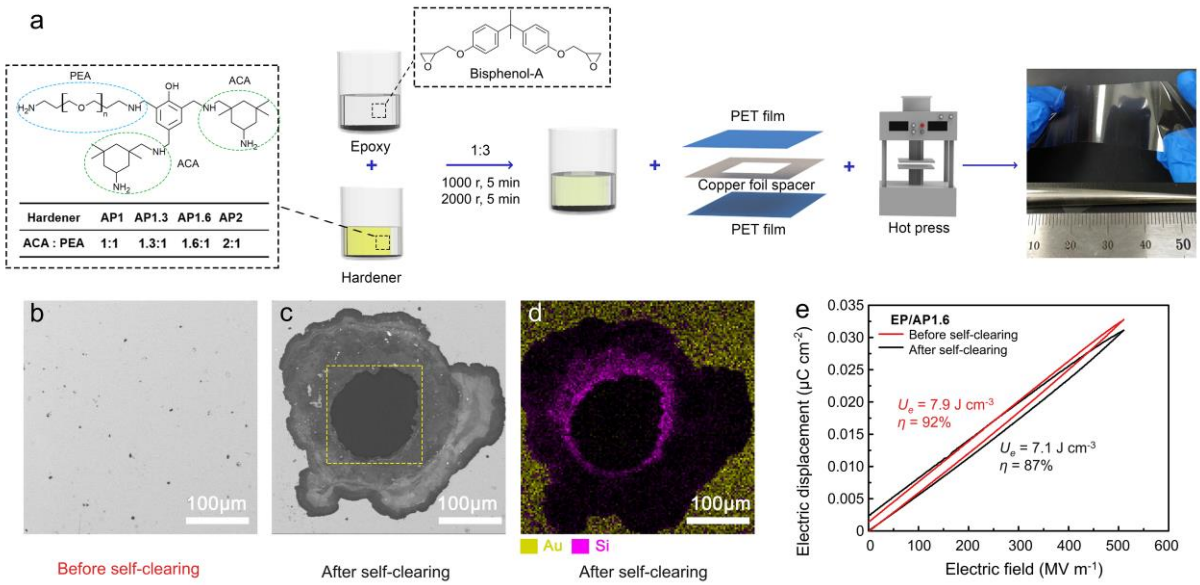

Fig. 16 (a) Schematic of epoxy resin film preparation. SEM images of the surface of epoxy film (b) before and (c) after self-clearing process. (d) EDS analysis of element distributions of the surface of epoxy film after self-clearing process (Au belongs to electrodes and Si comes from residues of silicone oil). (e) Unipolar *D*–*E* loops of epoxy films before and after self-clearing process measured at 510 MV m^{-1}.[104] Reproduced from ref. 104 with permission from Elsevier.

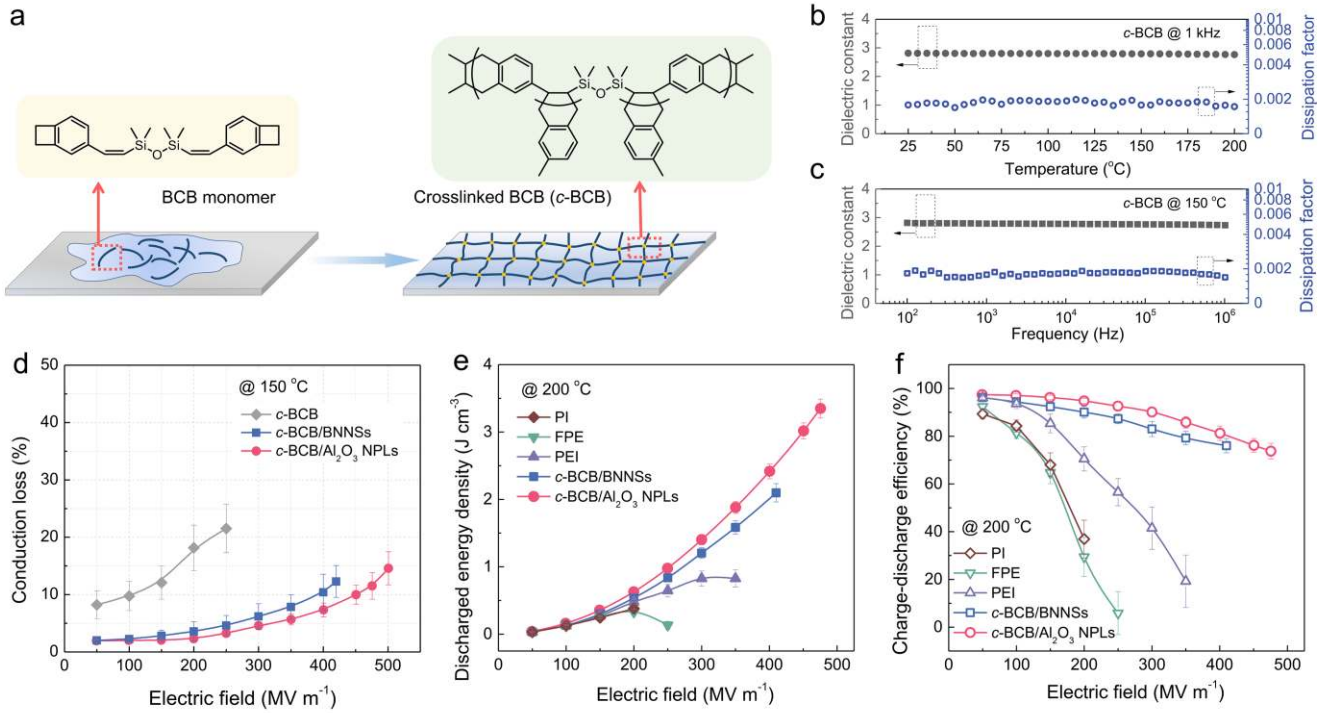

Fig. 17 (a) Schematic of the preparation of *c*-BCB films. (b) Temperature- and (c) Frequency-dependent dielectric spectra of *c*-BCB measured at 1 kHz and at 150 °C, respectively. (d) Conduction loss calculated from *D*–*E* loops of *c*-BCB, *c*-BCB/BNNSs (10 vol%) and *c*-BCB/Al_2O_3 NPLs (7.5 vol%) nanocomposites as a function of electric field at 150 °C. (e) Discharged energy density and (f) Charge-discharge efficiency of Kapton® PI, FPE, PEI and the *c*-BCB composites filled with 10 vol% BNNSs and 7.5 vol% Al_2O_3 NPLs measured at 200 °C, respectively.[67] Reproduced from ref. 67 with permission from John Wiley and Sons.

5.2. Crosslinking of thermoplastic dielectric polymers

In contrast to thermoset resins, thermoplastic polymers are melt-processable, which is compatible with the current fabrication techniques used for polymer film capacitors. The crosslinking of thermoplastic polymers has been proven to be very effective in improving the physical properties. For instance, the hardness, stiffness, wear and impact resistance, thermal stability and insulation strength are found to be synergistically increased through crosslinking of polyethylene to yield crosslinked polyethylene, which makes it an excellent insulation material widely used in high voltage power systems.[65,195] The crosslinking has also been demonstrated to improve the tensile stress, breakdown strength and capacitive performance of ferroelectric polymers.[196–198]

Khanchaitit *et al.* described a thermal crosslinking approach to reduce the ferroelectric hysteresis and conduction loss of poly(vinylidene fluoride-*co*-chlorotrifluoroethylene) (P(VDF-CTFE)) (15 wt% CTFE) under high electric fields.[198] The ferroelectric loss and conduction loss decrease from 18.5% and 37.3% of pristine polymer to 6.6% and 10.9% of the polymer network, respectively, at 350 MV m^{-1}, suggesting that the polar phase is destabilized and leakage current is impeded upon crosslinking. It was found that, in addition to the greatly decreased energy loss, the crosslinked ferroelectric polymers exhibit markedly improved E_b and electric polarization density as well as retain a high *K* of around 10 at 1 kHz, which give rise to high U_e and η (*e.g.*, 17 J cm^{-3} and 83% at 400 MV m^{-1} and room temperature). In addition, the crosslinking approach enhances the capacitive capability of the ferroelectric P(VDF-CTFE) at high temperatures. At 70 °C, the polymer networks deliver an U_e of 10 J cm^{-3}, whereas the melt-stretched commercial P(VDF-CTFE) normally breaks down at around 250 MV m^{-1} with an U_e of < 2 J cm^{-3}.

To further improve the operating temperature of fluoropolymers, more recently, Li *et al.* crosslinked poly(chlorotrifluoroethylene-*co*-vinylidene fluoride) (P(CTFE-VDF), 2.5 mol% VDF, abbreviated as VK) by melt-processing of the mixture of VK, dicumyl peroxide (DCP) as the initiator and triallyl isocyanurate (TAIC) as the co-agent as illustrated in Fig. 18a.[199] DCP thermally decomposes into peroxide radicals that abstract chlorine atoms from the CTFE unit to form macromolecular radicals, which are then reacted with TAIC to yield crosslinked VK (XL-VK) thin films. XL-VK-1 to XL-VK-3 correspond to the initiator concentration varying from 2, 3 and 4 wt% in the polymer networks. It is noteworthy that the presence of a small amount of vinylidene fluoride endows the facile moldability of VK, which is in sharp contrast to PTFE families as discussed in Section 3.1. While crosslinking has little effect on the dielectric properties at low electric fields, it significantly enhances the high-field dielectric properties and capacitive performance especially at elevated temperatures. For example, at 150 °C, the XL-VK displays an E_b of 494 MV m^{-1}, which represents a ~100% enhancement with respect to the pristine polymer (*i.e.*, 251 MV m^{-1}) (Fig. 18b). The remarkably improved high-temperature dielectric strength along with a relatively high *K* of 3.62 (at 1 kHz and 150 °C)

leads to the maximum U_e of 4.33 J cm^{-3} at 526 MV m^{-1} as shown in Fig. 18c. More impressively, the XL-VK film delivers ultrahigh η > 97.7% across a wide temperature range from 25 to 150 ℃ under 200 MV m^{-1}, far exceeding not only pristine VK but also the state-of-the-art BOPP and high-temperature dielectric polymers including Kapton® PI, FPE, PEI, as compared in Fig. 18d. The cyclic test operating at 150 ℃ and 200 MV m^{-1} shows no sign of degradation in U_e with < 1.2% variation over 50 000 charging–discharging cycles. The origins of the marked improvement in the high-temperature capacitive performance are traced to efficient charge-trapping by a range of molecular trapping centers created by the crosslinked structures as evidenced by the thermally stimulated depolarization current (TSDC) and pulsed electroacoustic (PEA) measurements. For instance, the trap energy level derived from TSDC curves increases from 0.57 eV of VK to the maximum value of 1.03 eV of the XL-VK, manifesting the higher energy barriers are introduced in the polymer networks upon crosslinking. As a result, as shown in Fig. 18e, the current density is suppressed by nearly two orders of magnitude and the calculated hopping distance is reduced by more than twice, *e.g.*, from 6.99×10^{-7} A cm^{-2} and 1.88 nm of VK to 1.14×10^{-8} A cm^{-2} and 0.92 nm of the XL-VK at 100 MV m^{-1} and 150 °C.

In addition to fluoropolymers, crosslinking has been demonstrated effective in improving E_b and enhancing electrical and mechanical stability of thermoplastic polymers with a high degree of aromaticity and fused-ring heterocyclic structures over a wide temperature range of 25–300 °C. PAEN has been thermally crosslinked to yield PAEN networks (*c*-PAEN) via a two-step procedure.[200] First, the PAEN networks terminated with phthalonitrile are achieved through the self-crosslinking between the cyano groups from the sidechain and the end of the main chain of PAEN. Second, the fully crosslinked PAEN films are obtained by a post-reaction between phthalocyanines and triazine rings. The *c*-PAEN prepared at 350 °C exhibits a greatly enhanced T_g of > 370 °C and an E_b of 188 MV m^{-1} at 300 °C.

Similarly, a crosslinked network was prepared based on 4-phenylethynylphthalic anhydride (PEPA)-terminated PEI (PEPA-PEI) oligomer synthesized from 2,2-bis[4-(3,4-dicarboxyphenoxy)phenyl] propane dianhydride (BPADA) and 4,4′-ODA as shown in Fig. 19a.[201] It was found that the PEPA-PEI oligomer can be thermally crosslinked to yield PEPA-PEI networks (*c*-PEPA-PEI) film under both oxygen and vacuum conditions at temperatures ranging from 300–320 °C (Fig. 19b). Interestingly, the *c*-PEPA-PEI prepared under oxygen at 320 °C delivers lower leakage current densities and higher capacitive performance, *e.g.*, an U_e of 3.6 J cm^{-3} measured at 150 °C and 100 Hz under an electric field of 500 MV m^{-1}, compared to the sample fabricated in the vacuum. It is inferred that the oxygen is involved in the crosslinking process and forms oxygen bridge bonds with phenylethynyl group (Fig. 19c), which yields the *c*-PEPA-PEI with enhanced thermal resistance and higher chain flexibility.

Briefly, the crosslinking of both thermoset and thermoplastic polymers has been studied for decades and proved to be a very

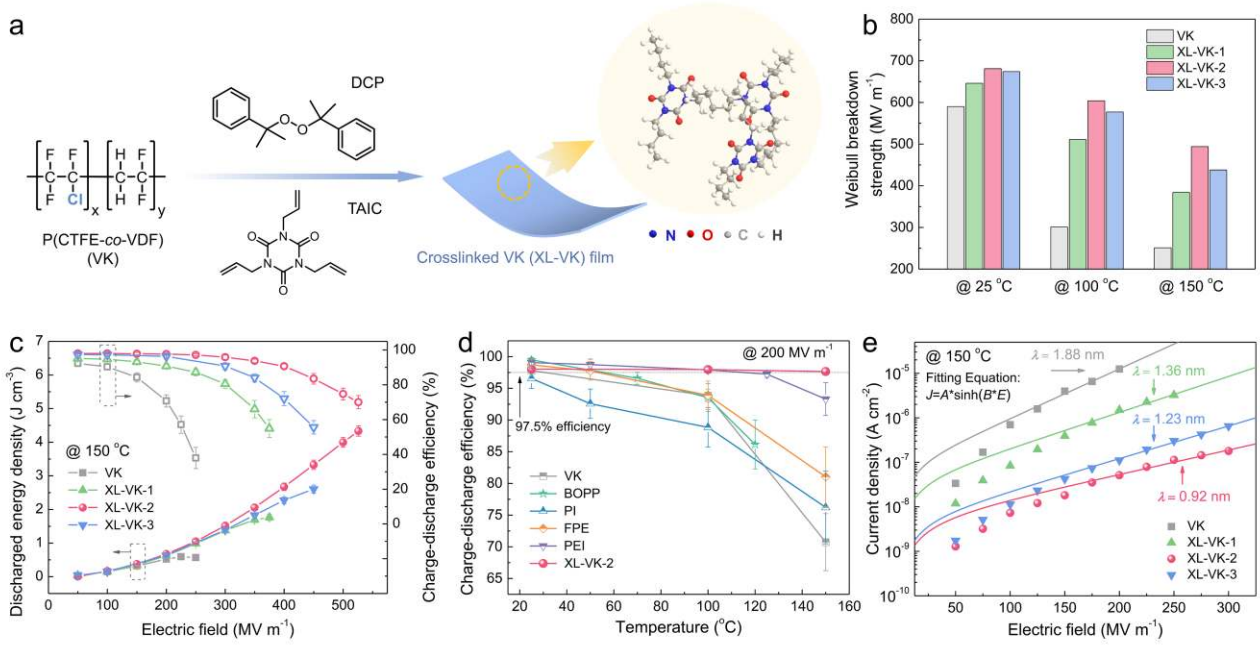

Fig. 18 (a) Schematic of the preparation of XL-VK films. (b) Weibull breakdown strength of VK and XL-VKs measured at 25 °C, 100 °C and 150 °C, respectively. (c) Discharged energy density and charge–discharge efficiency of VK and XL-VKs at 150 °C. (d) Charge–discharge efficiency of VK, BOPP, Kapton® PI, FPE, PEI and XL-VK-2 as a function of temperature measured at 200 MV m^{-1}. (e) Conduction current density of VK and XL-VKs as a function of electric field at 150 °C. Solid curves represent the fitting to hyperbolic sine.[199] Reproduced from ref. 199 with permission from The Royal Society of Chemistry.

effective means to improve multiple physical properties. The implementation of significantly improved high-temperature capacitive performance of polymers with the prospect of large-scale industrial application based on this molecular engineering approach

is very encouraging and deserves continuing attention. Particularly, the mild and controllable crosslinking condition with compatibility to current film capacitor fabrication techniques is highly desired. The influence of residuals and crosslinking byproducts along with the change in crystallinity and mechanical strength and its impact on high-temperature capacitive performance also requires comprehensive characterization and investigation.

6. Multicomponent assembly approach to high-temperature dielectric polymers

6.1. Dielectric polymer blends

To achieve high *K* in polymer dielectrics, it would necessitate the incorporation of large dipoles in polymer chains. However, the strong coupling between the dipoles introduces high hysteresis loss as evidenced in ferroelectric polymers.[202] On the other hand, while weakly coupled strong dipoles in polymers exhibit low tan δ, low *K* is seen at temperatures far below T_g because of the constrains of the glassy structure on the dipoles.[203,204] At temperatures above T_g, the reduced constrains on the dipoles as a result of the increased free volume would give rise to a large increase in *K*. However, the tan δ also becomes high at temperatures above T_g. Therefore, if free volume can be introduced in polymers with strongly coupled dipoles at a temperature far below T_g, a high *K* can be achieved without compromise on the tan δ.

The blending of two dissimilar polymers provides a facile but effective way to create partial mismatches between the two polymer chains, resulting in an increase in the interchain spacing and additional free volume in the glassy blend. Thus, the constraints and barriers for dipole orientation under the electric field are reduced in the glassy state to produce a high *K*. Zhang and coworkers blended two strongly polar polymers, *i.e.*, PEEU with a *K* of 4.7 and ArPTU with a *K* of 4.4.[205] As suggested by the DFT simulations, the mismatch of the polymer unit lengths and the locations of the dipolar functional groups cause complex interchain interaction between the two polymer chains, which slightly increases the free volume between the polymer chains (Fig. 20a). The expanded interchain spacing and free volume in the blend enables easier dipole reorientation and leads to a *K* of 7.5 while maintaining a tan δ of below 1% (Fig. 20b), which are stable with the temperature up to 120 °C (Fig. 20c). Another work by Zhang and coworkers suggests that the polymer blending strategy is also applicable to other high T_g dipolar polymers, *e.g.*, PEI and poly(ether-methyl-ether-urea) (PEMEU).[206] The PEI/PEMEU blend shows a high *K* of 5.8 and a low tan δ of below 1% over a wide temperature range up to 150 °C. The increased *K* in PEI/PEMEU blend is attributed to the disruption of hydrogen bonds and improved free volume for dipoles in the glassy state. However, up to date, only the low-field dielectric properties of the blends have been studied, the high-field capacitive performance, especially at high temperatures, remains to be evaluated.

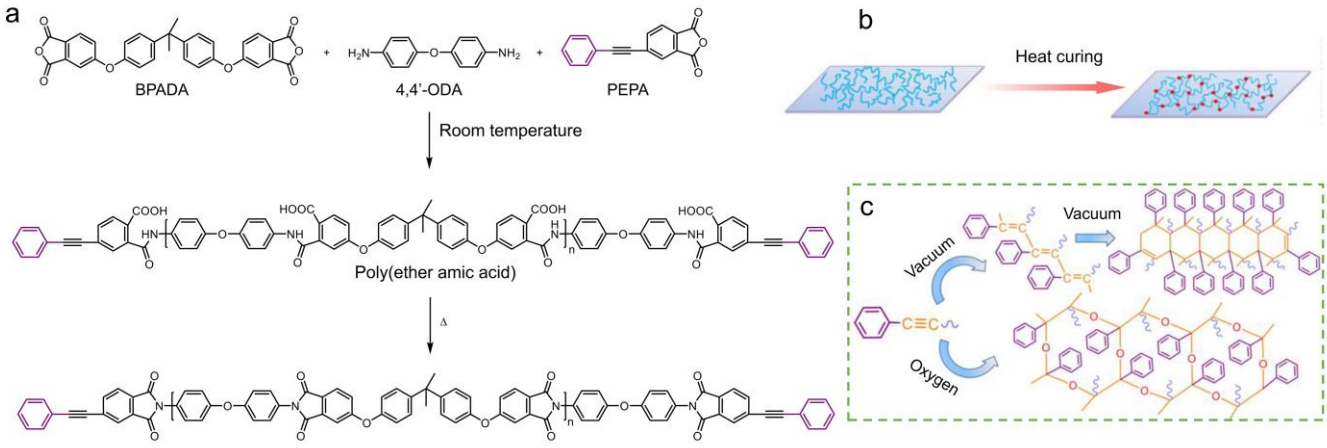

Fig. 19 (a) Synthetic scheme of phenylethynyl-terminated PEI oligomers. (b) Schematic of thermal crosslinking of *c*-PEPA-PEI film on the substrate. (c) The proposed curing reaction mechanism of phenylethynyl groups in vacuum and under oxygen atmosphere.[201] Reproduced from ref. 201 with open access from Chinese Chemical Society

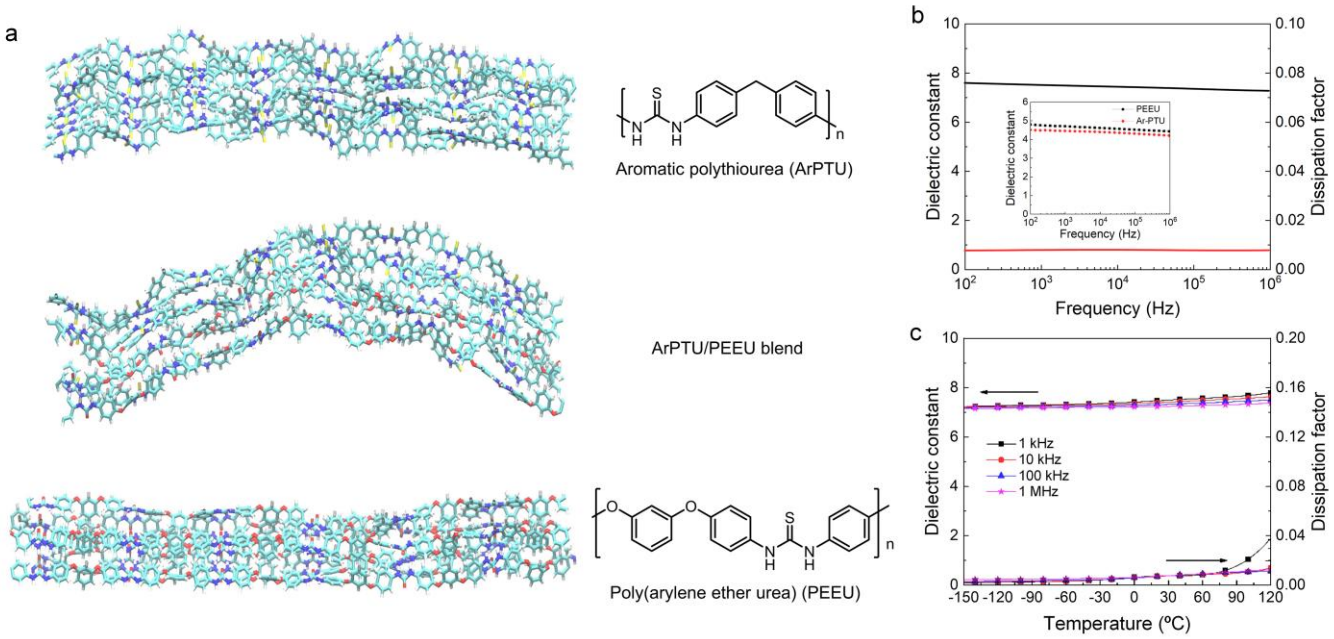

Fig. 20 (a) DFT simulated unit cell of ArPTU, PEEU/ArPTU blend and PEEU. (b) Frequency-dependent dielectric spectra of PEEU/ArPTU blend at room temperature. Inset, frequency-dependent dielectric constant of PEEU and ArPTU. (c) Temperature-dependent dielectric spectra of PEEU/ArPTU blend at various frequencies.[205] Reproduced from ref. 205 with permission from Elsevier.

To inhibit the charge injection and conduction, an all-organic polymer blend composed of high-temperature polymers and very low concentration (0.25–0.75 vol%) of organic high-electron-affinity molecular semiconductors was demonstrated.[207] The blend shows greatly enhanced capacitive energy storage performance at 200 ℃, which is very close to the T_g of the polymer (*i.e.*, 217 ℃). The organic high-electron-affinity molecular semiconductors introduce charge traps with a large trap energy level (Fig. 21a-c), which can effectively immobilize the injected and excited electrons via strong electrostatic attraction even under high temperatures and high applied fields.[208] The immobilized injected electrons near the electrode/dielectric interface would establish a built-in electric field opposite to the direction of the applied electric field,[209] which suppresses the further charge injection and decreases the Schottky emission conduction current (Fig. 21d-f). Moreover, the deep traps inhibit the charge transport in the bulk of the dielectric film to suppress the hopping conduction current.[64] The maximum U_e obtained at η > 90% in PEI/[6,6]-phenyl C61 butyric acid methyl ester (PEI/PCBM) blend is 4.5 J cm^{-3} at 150 ℃ (Fig. 21g), whereas U_e of pristine PEI is only 1.0 J cm^{-3}. At 200 ºC, an U_e of 3 J cm^{-3} and a high η of 90% is achieved in the blend (Fig. 21h), which outperforms state-of-the-art high temperature polymer-based dielectrics (Fig. 21i). Compared to organic/inorganic composites, the all-organic polymer/molecular semiconductor blend presents advantages in large-scale processability and facile control of film quality owing to the high miscibility of the organic molecular semiconductors and polymer dielectrics. Impressively, the molecular semiconductor-doped PEI exhibits cyclability outperforming pristine PEI and PEI/inorganic nanofiller composites in 50 000-time charging–discharging tests at 200 °C and 200 MV m^{-1}, indicative of superior long-term reliability of all-organic polymer blend films.

6.2. Multi-layered dielectric polymers

In dielectric polymer blends with randomly dispersed phases, it remains challenging to precisely manage the interfacial polarization. By contrast, in the layered polymer films, the interfacial polarization can be rationally designed and facilely utilized to further improve the electrical polarization and breakdown strength, and reduce the energy loss of polymer dielectrics.[203,210,211] Using multilayer coextrusion technology (Fig. 22a),[210] Zhu *et al*. developed various multi-layered polymer films composed of alternating layers of a high-breakdown-strength linear dielectric polymer (*e.g.*, PC, PET and polysulfone (PSF)) and a high-*K* ferroelectric polymer (*e.g.*, PVDF and its copolymers).[212–216] As shown in Fig. 22b, the layer thickness and composition of the PC/PVDF multi-layered polymer films can be readily adjusted in the extrusion process.[212] Due to the large contrast in *K* and conductivity of PC and PVDF, space charges and impurity ions are accumulated at the multilayer interfaces, which can block the charge migration, thus reducing the dielectric loss from the ion-hopping (Fig. 22c).[202] As shown in the dielectric spectra of PC/PVDF

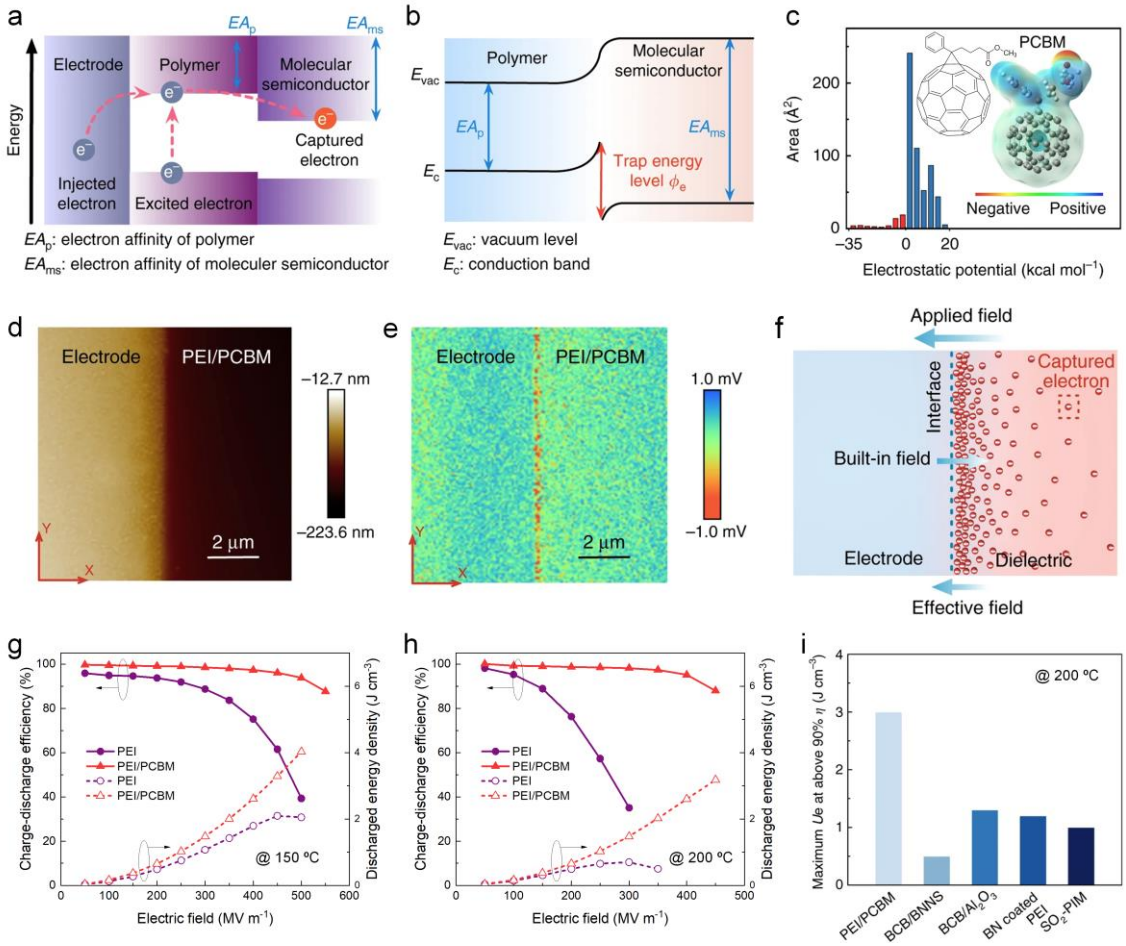

Fig 21 (a) Band diagram of the possible charge transfer process. (b) Schematic of trap energy level introduced by the molecular semiconductor in dielectric polymers. (c) Electrostatic potential distribution and area percentage in each electrostatic potential range of PCBM. (d) Topography of the PEI/PCBM composite. (e) Surface potential mapping of the PEI/PCBM composite. (f) Schematic of the built-in electric field formed by the molecular semiconductor captured electrons. Field-dependent discharged energy density and charge–discharge efficiency of PEI and PEI/PCBM blend at (g) 150 °C and (h) 200 °C, respectively. (i) Comparison of the maximum discharged energy density at above 90% efficiency between the PEI/PCBM and the state-of-the-art high-temperature polymer dielectrics at 200 °C.[207] Reproduced from ref. 207 with open access from Springer Nature.

multi-layered polymer films at 75 ℃, the relaxation peak at 0.05 Hz, which corresponds to impurity ion-hopping polarization, gradually decreases with the increase of the layer number (*i.e.*, decreased layer thickness), indicating that the nanoconfinement effect plays an important role in tailoring the dielectric properties of the multi-layered polymer films (Fig. 22d).[212] Moreover, the interfacial charges can act as effective traps to block the charge injection from the electrode and charge migration in the multi-layered films, thereby enhancing the breakdown strength. The PC/PVDF and PC/nylon multi-layered polymer films show stable capacitive energy storage performance at about 125 ℃ (Fig. 22e-f).[213] The thermal stability of the multi-layered polymer films can be extended up to 150 ℃ when using high T_g polymers, such as PC and PSF.[217] To further suppress the conduction loss, the multi-layered films can be poled at a temperature slightly below the T_g of the linear dielectrics to driven the impurity ions into the linear dielectrics layers and then block them after cooling.[218] It should be noted that interfacial adhesion between the immiscible polymer layers is very important to achieve improved capacitive performance in multi-layered polymer films.

Previous studies on the conduction mechanism of high-temperature polymer dielectrics indicate that Schottky emission is responsible for the majority of the conduction current under high electric fields and high temperatures.[17,62,68,155,219] To suppress the Schottky emission conduction current, the energy barrier at the electrode/dielectric interfaces should be improved. Accordingly, the surface of the high-temperature dielectric polymer films have been

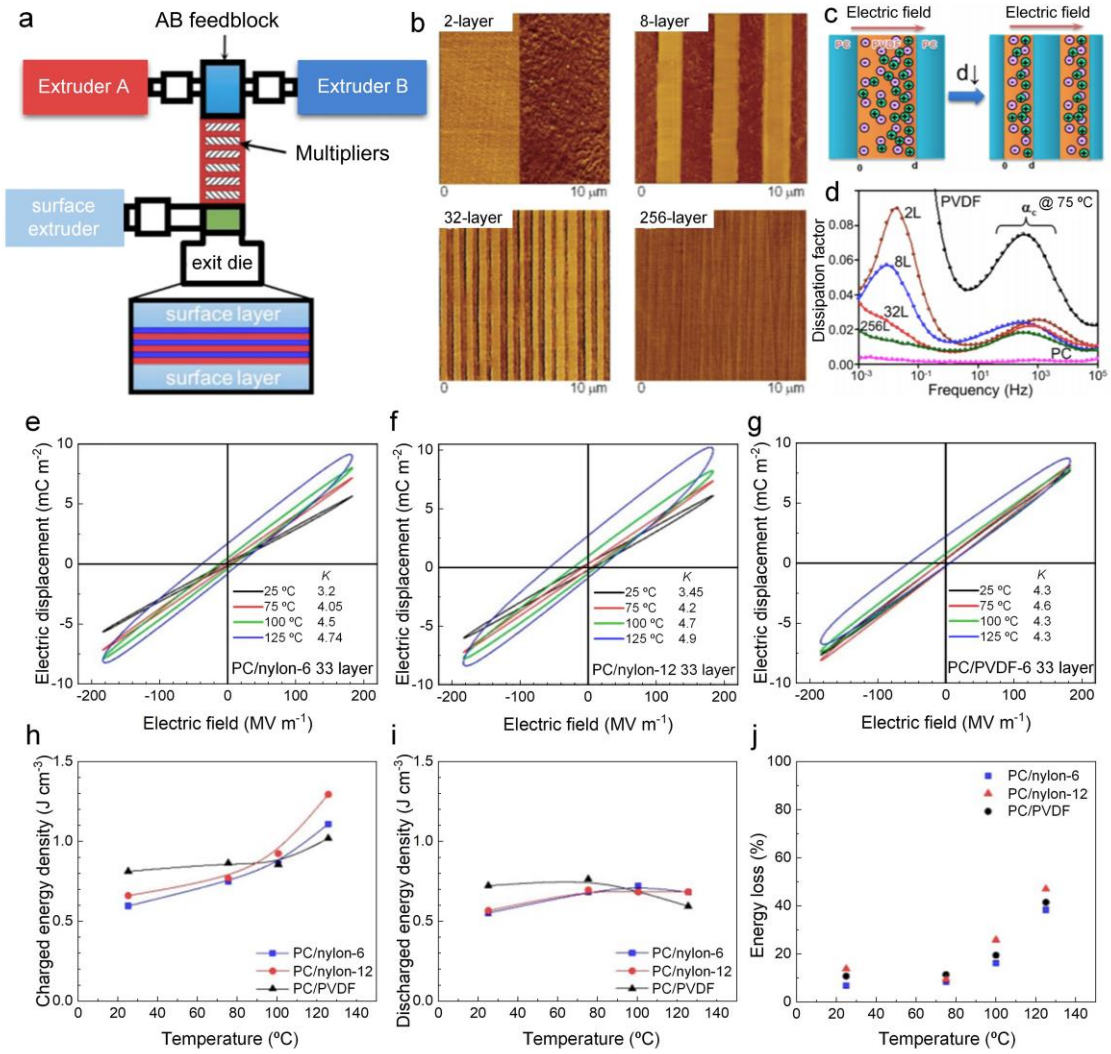

Fig. 22 (a) Schematic of the coextrusion process of the multi-layered polymer dielectrics.[210] (b) Atomic force microscope (AFM) phase images of PC/PVDF 50/50 (vol/vol) multi-layered films with different layers: 2-layer, 8-layer, 32-layer and 256-layer. (c) Schematic of the nanoconfinement effect on the ion-hopping polarization in PVDF layers with different thicknesses. (d) Frequency-dependent dissipation factor of the PC/PVDF 50/50 (vol/vol) multi-layered films with different layers and PVDF and PC control films at 75 °C.[212] Bipolar *D*–*E* loops of (e) PC/nylon-6, (f) PC/nylon-12 and (g) PC/PVDF 50/50 (vol/vol) 33-layer films at 25 °C, 75 °C, 100 °C, and 125 °C, respectively. Temperature-dependent (h) charged energy density, (i) discharged energy density and (j) energy loss of PC/nylon-6, PC/nylon-12, PC/PVDF 50/50 (vol/vol) 33-layer films, respectively.[213] Reproduced from ref. 210, ref. 212 and ref. 213 with permission from American Chemical Society.

coated with a wide bandgap inorganic layer with nanometer-scale thickness to increase the energy barrier at the electrode/dielectric interface and thus reduce the high-temperature conduction current.[17,155]

Upon the combination of different organic components with complementary functionalities, the high-temperature dielectric films based on polymer blends and multilayered polymer assemblies have been demonstrated very effective in improving high-temperature capacitive energy storage performance, especially in impeding electrical conduction under elevated electric fields. Nevertheless, the underlying mechanism of the enhanced dielectric properties needs to be further investigated. Advanced characterization techniques and theoretical tools are critically needed to gain fundamental insights into the organic-organic interface of the multicomponent-assembled polymer films. The structure-composition correlation is also worthy of a more in-depth investigation to provide scientific guidance on the rational selection of organic components.

7. Conclusions and outlook

The dielectric polymers are anticipated to be the material of choice to meet the booming demands for electrical power and electrification in the harsh environment. While exciting

elevated-temperature capacitive performance has been recently achieved in the dielectric polymer composites embedded with inorganic fillers, the composites are usually prepared by time-consuming methods involving multiple steps that are incompatible with the current melt-extrusion processes used for polymer dielectrics. Moreover, the precise control of uniformity and thickness of large-scale composite films remains an open question. In contrast, the dielectric polymers, when designed properly, can be melt-processed or fabricated by using other high throughput methods for film scale-up, thus presenting great scalability and allowing accurate control of film quality and reduction of film thickness to a few micro-meters. However, the current dielectric polymers still fall significantly short of meeting all the specifications for high-temperature capacitive energy storage applications, including U_e, η, E_b, charging–discharging cyclability, reliability and self-clearing capability.

To obtain excellent dielectric stability at high temperatures, most high-temperature dielectric polymers are designed based on the criteria of high-performance engineering polymers, such as containing aromatic or heteroaromatic backbones. Unfortunately, the conjugated planar segments may inevitably compromise the capacitive performance of the polymer dielectrics because of the significant conduction loss caused by the large charge carrier mobility along with the (hetero)aromatic segments. The aromatic or heteroaromatic backbones may also have adverse effects on the self-clearing capability of the metallized films because of the high carbon ratio in the structures. Additionally, high rigidity of the aromatic or heteroaromatic backbones may introduce difficulties in melt-processing of the polymers into high-quality thin films. PTFE is a highly promising polymer dielectric for high-temperature capacitive applications owing to its excellent temperature stability and ultra-low tan δ. Special attention needs to be paid to PTFE film processing because of the high melting viscosity of PTFE. In addition, the adhesion and reliability of the metal electrodes on PTFE films need to be optimized due to the low surface energy of fluorinated polymers.

The abruptly increased conduction current governed by various temperature- and electric field-dependent conduction mechanisms is well-recognized to be the major loss mechanism of polymer dielectrics at elevated temperatures and high fields and critically determines the high-temperature capacitive performance. High-T_g polymer dielectrics do not necessarily possess the high E_b and excellent η values at high temperatures unless the conduction current is effectively suppressed. To suppress the conduction current, the conduction mechanism of polymers over a wide temperature and electric field range should be comprehensively studied to gain fundamental insight into the conduction process and provide scientific guidance on the material design of high-temperature polymer dielectrics. Increasing the energy barrier at the dielectric polymer/electrode interface and introducing deep charge traps are the effective methods to inhibit the electrode-limited and bulk-limited conduction process, respectively. The surface functionalization of the polymer dielectrics by coating wide-bandgap functional layers can be readily applied to a variety of the currently available high-T_g polymers to significantly improve their high-temperature capacitive performance, which should draw continued attention. The crosslinked dielectric polymers exhibit enhanced elevated-temperature U_e and η up to 150 °C as a consequence of introduced deep charge traps resulting from crosslinking. However, it remains unclear whether the organic structure-based traps have sufficient energy levels against detrapping of charges at temperatures above 150 °C. The addition of a small amount of charge trapping moieties into high-T_g polymers is another promising approach worthy of intensive investigation.

While the current research focuses on the inhibition of high-field conduction loss, the improvement of K values, and consequently, U_s of high-temperature polymer dielectrics has received much less attention. The current high-temperature polymer dielectrics are mostly linear dielectrics with low K, *i.e.*, usually below 4, which severely limits their U_s. The grafting of polar groups onto the backbone or side chains of polymers has been shown to increase K and U_s of polymer dielectrics operating at room temperature. The increase in K is usually accompanied by high tan δ at ambient temperatures. With increasing temperature, high K may give rise to additional energy loss at high fields. Novel design and synthesis strategies are thus needed to improve K and U_s, while maintaining low loss at high fields and elevated temperatures. Engineering the topological structures by constructing multi-layered polymer dielectrics with different functional layers, *e.g.*, high-K layer and high-electrical-resistance layer, is attractive. The structure-property relationships in these complex polymer dielectrics deserve systematic investigation.

Although many scientific and technical challenges remain to be overcome, polymer dielectrics have shown great potential in harsh-environment capacitive energy storage applications. The remarkable progress of significantly improved high-temperature capacitive performance has been made in polymer dielectrics based on various structural design approaches during the past decade. Novel molecular design of the structures of polymer dielectrics should be performed to balance dielectric stability, low conduction and dielectric loss, and high K at elevated temperatures and high fields and realize superior energy and power densities. A systematic study of structure-dependent high-temperature electrical conduction mechanisms, dielectric properties and capacitive performance should be carried out. More critically, future research shall be devoted to the investigation of the structure-dependent graceful failure mechanism of polymer dielectrics at both ambient and high temperatures. In fact, the graceful failure mechanism has received the least attention in current research of polymer dielectrics. The graceful failure behavior actually plays an essential role in determining the applicability of all the newly developed polymer dielectrics in practical energy applications. Considerable investigations are required to examine and improve the fault resistance and the reliability of polymer dielectrics operating under extreme conditions. Theoretical modeling at multiple scales and advanced nanoscale imaging may help to further our understandings of the failure and self-clearing mechanisms of polymer dielectrics

at different operation conditions. Machine learning algorithms and existing materials data can be utilized to create surrogate models of dielectric/electrical properties and capacitive performance predictions. Computational and data sciences can accelerate the rational design of polymer structures and synthetic schemes. Rapid advances in a highly interdisciplinary field such as polymer dielectrics are to be expected only through collaborative efforts across the boundaries of chemistry, materials science and engineering, electrical engineering and applied physics.

Conflicts of interest

There are no conflicts to declare.

Acknowledgements

The work at The Pennsylvania State University was supported by the U.S. Office of Naval Research. The work at Lawrence Berkeley National Laboratory was supported by the U.S. Department of Energy, Office of Science, Office of Basic Energy Sciences, Materials Sciences and Engineering Division, under contract no. DE-AC02-05CH11231 within the Inorganic/Organic Nanocomposites Program (KC3104). H.L. thanks Z.L. Xie for discussion on figure design and preparation. Y.L. acknowledges the support from the Molecular Foundry, Lawrence Berkeley National Laboratory, a user facility supported by the Office of Science, Office of Basic Energy Sciences, of the U.S. Department of Energy under contract no. DE-AC02-05CH11231.

References

1 M. S. Dresselhaus and I. L. Thomas, *Nature*, 2001, **414**, 332–337.
2 H. Chen, T. N. Cong, W. Yang, C. Tan, Y. Li and Y. Ding, *Prog. Nat. Sci.*, 2009, **19**, 291–312.
3 T. M. Gür, *Energy Environ. Sci.*, 2018, **11**, 2696–2767.
4 M. M. Thackeray, C. Wolverton and E. D. Isaacs, *Energy Environ. Sci.*, 2012, **5**, 7854–7863.
5 X. Lin, M. Salari, L. M. R. Arava, P. M. Ajayan and M. W. Grinstaff, *Chem. Soc. Rev.*, 2016, **45**, 5848–5887.
6 Q. Li, L. Chen, M. R. Gadinski, S. Zhang, G. Zhang, H. U. Li, E. Iagodkine, A. Haque, L. Q. Chen, T. N. Jackson and Q. Wang, *Nature*, 2015, **523**, 576−579.
7 N. Meng, X. Ren, G. Santagiuliana, L. Ventura, H. Zhang, J. Wu, H. Yan, M. J. Reece and E. Bilotti, *Nat. Commun.*, 2019, **10**, 4535.
8 P. Simon and Y. Gogotsi, *Nat. Mater.*, 2008, **7**, 845–854.
9 J. W. Choi and D. Aurbach, *Nat. Rev. Mater.*, 2016, **1**, 16013.
10 F. Zhang, T. Zhang, X. Yang, L. Zhang, K. Leng, Y. Huang and Y. Chen, *Energy Environ. Sci.*, 2013, **6**, 1623–1632.
11 T. Christen and M. W. Carlen, *J. Power Sources*, 2000, **91**, 210–216.
12 B. Dunn, H. Kamath and J. M. Tarascon, *Science*, 2011, **334**, 928–935.
13 Y. Shao, M. F. El–Kady, J. Sun, Y. Li, Q. Zhang, M. Zhu, H. Wang, B. Dunn and R. B. Kaner, *Chem. Rev.*, 2018, **118**, 9233–9280.
14 C. Liu, Z. Yu, D. Neff, A. Zhamu and B. Z. Jang, *Nano Lett.*, 2010, **10**, 4863–4868.
15 E. J. Barshaw, J. White, M. J. Chait, J. B. Cornette, J. Bustamante, F. Folli, D. Biltchick, G. Borelli, G. Picci and M. Rabuffi, *IEEE Trans. Magn.*, 2006, **43**, 223–225.
16 M. Rabuffi and G. Picci, *IEEE Trans. Plasma Sci.*, 2002, **30**, 1939–1942.
17 Y. Zhou, Q. Li, B. Dang, Y. Yang, T. Shao, H. Li, J. Hu, R. Zeng, J. L. He and Q. Wang, *Adv. Mater.*, 2018, **30**, 1805672.
18 J. P. Zheng and T. R. Jow, *J. Power Sources*, 1996, **62**, 155–159.
19 T. Kousksou, P. Bruel, A. Jamil, T. El Rhafiki and Y. Zeraouli, *Sol. Energy Mater. Sol. Cells*, 2014, **120**, 59–80.
20 S. Ducharme, *ACS Nano*, 2009, **3**, 2447–2450.
21 B. Chu, X. Zhou, K. Ren, B. Neese, M. Lin, Q. Wang, F. Bauer and Q. M. Zhang, *Science*, 2006, 313, 334–336.
22 Q. Li, K. Han, M. R. Gadinski, G. Zhang and Q. Wang, *Adv. Mater.*, 2014, **26**, 6244–6249.
23 K. M. Slenes, P. Winsor, T. Scholz and M. Hudis, *IEEE Trans. Magn.*, 2001, **37**, 324–327.
24 I. R. McNab, *IEEE Trans. Plasma Sci.*, 2014, **42**, 1118–1127.
25 D. Tan, L. Zhang, Q. Chen and P. Irwin, *J. Electron. Mater.*, 2014, **43**, 4569–4575.
26 Global Power Capacitor Markets in 2020: Expect Slow and Steady Market Growth, https://www.tti.com/content/ttiinc/en/resources/marketeye/categories/passives/me–zogbi–20200309.html, (accessed September 2020).
27 H. Palneedi, M. Peddigari, G. T. Hwang, D. Y. Jeong and J. Ryu, *Adv. Funct. Mater.*, 2018, **28**, 1803665.
28 Z. Yao, Z. Song, H. Hao, Z. Yu, M. Cao, S. Zhang, M. T. Lanagan and H. Liu, *Adv. Mater.*, 2017, **29**, 1601727.
29 H. Pan, F. Li, Y. Liu, Q. H. Zhang, M. Wang, S. Lan, Y. P. Zheng, J. Ma, L. Gu, Y. Shen, P. Yu, S. J. Zhang, L. Q. Chen, Y. H. Lin and C. W. Nan, *Science*, 2019, **365**, 578–582.
30 G. Wang, J. Li, X. Zhang, Z. Fan, F. Yang, A. Feteira, D. Zhou, D. C. Sinclair, T. Ma, X. Tan, D. Wang and I. M. Reaney, *Energy Environ. Sci.*, 2019, **12**, 582–588.
31 F. Z. Yao, Q. Yuan, Q. Wang and H. Wang, *Nanoscale*, 2020, **12**, 17165–17184.
32 H. Li, F. Liu, B. Fan, D. Ai, Z. Peng and Q. Wang, *Small Methods*, 2018, **2**, 1700399.
33 Y. Wang, J. Chen, Y. Li, Y. Niu, Q. Wang and H. Wang, *J. Mater. Chem. A*, 2019, **7**, 2965–2980.
34 Q. Li, G. Zhang, F. Liu, K. Han, M. R. Gadinski, C. Xiong and Q. Wang, *Energy Environ. Sci.*, 2015, **8**, 922–931.
35 M. Guo, J. Jiang, Z. Shen, Y. Lin, C. W. Nan and Y. Shen, *Mater. Today*, 2019, **29**, 49–67.
36 X. Huang and P. Jiang, *Adv. Mater.*, 2015, **27**, 546–554.
37 Z. M. Dang, J. K. Yuan, J. W. Zha, T. Zhou, S. T. Li and G. H. Hu, *Prog. Mater. Sci.*, 2012, 57, 660–723.
38 H. Luo, X. Zhou, C. Ellingford, Y. Zhang, S. Chen, K. Zhou, D. Zhang, C. R. Bowen and C. Wan, *Chem. Soc. Rev.*, 2019, **48**, 4424–4465.
39 G. F. Mansbridge, *J. Inst. Electr. Eng.*, 1908, **41**, 535−564.
40 S. A. Boggs, J. Ho and T. R. Jow, *IEEE Electr. Insul. Mag.*, 2010, **26**, 7−13.
41 Y. Chen, H. Li, F. Lin, F. Lv, M. Zhang, Z. Li and D. Liu, *IEEE Trans. Plasma Sci.*, 2012, **40**, 2014−2019.
42 Z. M. Dang, J. K. Yuan, S. H. Yao and R. J. Liao, *Adv. Mater.*, 2013, **25**, 6334−6365.
43 Q. Wang and L. Zhu, *J. Polym. Sci. B Polym. Phys.*, 2011, **49**, 1421–1429.
44 J. Wei and L. Zhu, *Prog. Polym. Sci.*, 2020, **106**, 101254.
45 Y. Qiao, X. Yin, T. Zhu, H. Li and C. Tang, *Prog. Polym. Sci.*, 2018, **80**, 153−162.
46 W. Xia and Z. Zhang, *IET Nanodielectr.*, 2018, **1**, 17−31.
47 Q. Li, F. Z. Yao, Y. Liu, G. Zhang, H. Wang and Q. Wang, *Annu. Rev. Mater. Res.*, 2018, **48**, 219−243.
48 J. S. Ho and S. G. Greenbaum, *ACS Appl. Mater. Interfaces*, 2018, **10**, 29189−29218.

49 C. Buttay, D. Planson, B. Allard, D. Bergogne, P. Bevilacqua, C. Joubert, M. Lazar, C. Martin, H. Morel, D. Tournier and C. Raynaud, *Mater. Sci. Eng., B*, 2011, **176**, 283−288.
50 R. W. Johnson, J. L. Evans, P. Jacobsen, J. R. Thompson and M. Christopher, *IEEE Trans. Electron. Packag.*, 2004, **27**, 164−176.
51 K. Bennion and M. Thornton, presented at SAE World Cong., Detroit, April, 2010.
52 J. A. Weimer, Electrical power technology for the more electric aircraft, *AIAA/IEEE Dig. Avion. Syst. Conf.*, IEEE, 1993.
53 J. Watson and G. Castro, *J. Mater. Sci.: Mater. Electron.*, 2015, **26**, 9226–9235.
54 P. G. Neudeck, R. S. Kojie and L. Y. Chen, *Proc. IEEE*, 2002, **90**, 1065–1076.
55 J. Watson and G. Castro, *Analog Dialogue*, 2012, **46**, 1–7.
56 S. Zhang, C. Zou, D. I. Kushner, X. Zhou, R. J. Orchard Jr., N. Zhang and Q. M. Zhang, *IEEE Trans. Dielectr. Electr. Insul.*, 2012, **19**, 1158–1166.
57 D. Montanari, K. Saarinen, F. Scagliarini, D. Zeidler, M. Niskala and C. Nender, Film Capacitors for Automotive and Industrial Applications, *CARTS Proceedings*, 2009.
58 B. Fan, F. Liu, G. Yang, H. Li, G. Zhang, S. Jiang and Q. Wang, *IET Nanodielectr.*, 2018, **1**, 32–40.
59 D. Q. Tan, *Adv. Funct. Mater.*, 2020, **30**, 1808567.
60 N. Pfeiffenberger, F. Milandou, M. Niemeyer, T. Sugawara, M. Sanner and J. Mahood, *IEEE Trans. Dielectr. Electr. Insul.*, 2018, **25**, 120–126.
61 D. Ai, H. Li, Y. Zhou, L. Ren, Z. Han, B. Yao, W. Zhou, L. Zhao, J. Xu and Q. Wang, *Adv. Energy Mater.*, 2020, **10**, 1903881.
62 S. Cheng, Y. Zhou, J. Hu, J. L. He and Q. Li, *IEEE Trans. Dielectr. Electr. Insul.*, 2020, **27**, 498–503.
63 J. Ho and T. R. Jow, *IEEE Trans. Dielectr. Electr. Insul.*, 2012, **19**, 990–995.
64 Y. Zhou, C. Yuan, C. Li, P. Meng, J. Hu, Q. Li and J. L. He, *IEEE Trans. Dielectr. Electr. Insul.*, 2019, **26**, 1596–1604.
65 Y. Zhou, S. Peng, J. Hu and J. L. He, *IEEE Trans. Dielectr. Electr. Insul.*, 2017, **24**, 1308–1318.
66 J. M. Yang, X. Wang, C. J. Zheng, H. Zhao and Q. Q. Lei, DC Conduction Properties of SiO_2/LDPE Nanocomposite, *IEEE Int'l. Conf. Properties Applications Dielectr. Mater.* (*ICPADM*), IEEE, 2012.
67 H. Li, D. Ai, L. Ren, B. Yao, Z. Han, Z. Shen, J. Wang, L. Q. Chen and Q. Wang, *Adv. Mater.*, 2019, **31**, 1900875.
68 Q. Li, F. Liu, T. Yang, M. R. Gadinski, G. Zhang, L. Q. Chen and Q. Wang, *Proc. Natl. Acad. Sci. USA*, 2016, **113**, 9995–10000.
69 H. Li, L. Ren, D. Ai, Z. Han, Y. Liu, B. Yao and Q. Wang, *InfoMat*, 2020, **2**, 389–400.
70 H. Li, Z. Xie, L. Liu, Z. Peng, Q. Ding, L. Ren, D. Ai, W. Reainthippayasakul, Y. Huang and Q. Wang, *IEEE Trans. Dielectr. Electr. Insul.*, 2019, **26**, 722–729.
71 L. Ren, L. Yang, S. Zhang, H. Li, Y. Zhou, D. Ai, Z. Xie, X. Zhao, Z. Peng, R. Liao and Q. Wang, *Compos. Sci. Technol.*, 2021, **201**, 108528.
72 Y. Zhou, C. Yuan, S. Wang, Y. Zhu, S. Cheng, X. Yang, Y. Yang, J. Hu, J. L. He and Q. Li, *Energy Storage Mater.*, 2020, **28**, 255–263.
73 M. Fan, P. Hu, Z. Dan, J. Jiang, B. Sun and Y. Shen, *J. Mater. Chem. A*, 2020, **8**, 24536–24542.
74 W. Ren, J. Pan, Z. Dan, T. Zhang, J. Jiang, M. Fan, P. Hu, M. Li, Y. Lin, C. W. Nan and Y. Shen. *Chem. Eng. J.*, 2020, DOI: 10.1016/j.cej.2020.127614.
75 W. Xu, J. Liu, T. Chen, X. Jiang, X. Qian, Y. Zhang, Y. Zhang and Z. Jiang, *Small*, 2019, **15**, 1901582.
76 H. Li, L. Ren, Y. Zhou, B. Yao and Q. Wang, *High Volt.*, 2020, **5**, 365–376.
77 S. L. Zhong, Z. M. Dang, W. Y. Zhou and H. W. Cai, *IET Nanodielectr.*, 2018, **1**, 41–47.
78 Q. Li and S. Cheng, *IEEE Electr. Insul. Mag.*, 2020, **36**, 7–28.
79 Y. Zhou and Q. Wang, *J. Appl. Phys.*, 2020, **127**, 240902.
80 B. Fan, M. Zhou, C. Zhang, D. He and J. Bai, *Prog. Polym. Sci.*, 2019, **97**, 101143.
81 V. K. Thakur and R. K. Gupta, *Chem. Rev.*, 2016, **116**, 4260–4317.
82 S. Park, C. H. Kim, W. J. Lee, S. Sung and M. H. Yoon, *Mater. Sci. Eng. R Rep.*, 2017, **114**, 1–22.
83 S. O. Kasap, Principles of Electronic Materials and Devices, McGraw Hill Education, 2007.
84 C. C. Wang, G. Pilania, S. A. Boggs, S. Kumar, C. Breneman and R. Ramprasad, *Polymer*, 2014, **55**, 979–988.
85 C. W. Nan, Y. Shen and J. Ma, *Annu. Rev. Mater. Res.*, 2010, **40**, 131–151.
86 X. Huang, B. Sun, Y. Zhu, S. Li and P. Jiang, *Prog. Mater. Sci.*, 2019, **100**, 187–225.
87 K. C. Kao, *Dielectric Phenomena in Solids*, Academic Press, 2004.
88 T. Blythe and D. Bloor, *Electrical Properties of Polymers*, Cambridge University Press, 2005.
89 M. Ieda, *IEEE Trans. Electr. Insul.*, 1980, **EI–15**, 206–224.
90 D. Q. Tan, *J. Appl. Polym. Sci.*, 2020, **137**, 49379.
91 M. Ieda, *IEEE Trans. Electr. Insul.*, 1984, **EI–19**, 162–178.
92 M. Huang, Y. Zhou, Z. Zhou and B. Qi, *Energies*, 2017, **10**, 2160.
93 L. A. Dissado, T. C. Fothergill, S. V. Wolfe and R. M. Hill, *IEEE Trans. Electr. Insul.*, 1984, **EI–19**, 227–233.
94 F. C. Chiu, *Adv. Mater. Sci. Eng.*, 2014, **2014**, 578168.
95 B. X. Du, C. Han, J. Li and Z. Lei, *IEEE Trans. Dielectr. Electr. Insul.*, 2020, **27**, 418–426.
96 V. Ambegaokar, B. I. Halperin and J. S. Langer, *Phys. Rev. B*, 1971, **4**, 2612.
97 J. G. Simmons, *Phys. Rev.*, 1967, **155**, 657.
98 G. Lengyel, *J. Appl. Phys.*, 1966, **37**, 807–810.
99 Q. Chen, Y. Wang, X. Zhou, Q. M. Zhang and S. Zhang, *Appl. Phys. Lett.*, 2008, **92**, 142909.
100 Q. Chen, Y. Shen, S. Zhang and Q. M. Zhang, *Annu. Rev. Mater. Res.*, 2015, **45**, 433–458.
101 Q. M. Zhang, V. Bharti and X. Zhao, *Science*, 1998, **280**, 2101–2104.
102 L. Zhu and Q. Wang, *Macromolecules*, 2012, **45**, 2937–2954.
103 P. Yang, F. Tian and Y. Ohki, *IEEE Trans. Dielectr. Electr. Insul.*, 2014, **21**, 2310–2317.
104 S. Chen, G. Meng, B. Kong, B. Xiao, Z. Wang, Z. Jing, Y. Gao, G. Wu, H. Wang and Y. Cheng, *Chem. Eng. J.*, 2020, **387**, 123662.
105 C. W. Reed and S. W. Cichanowskil, *IEEE Trans. Dielectr. Electr. Insul.*, 1994, **1**, 904–922.
106 D. G. Shaw, S. W. Cichanowski and A. Yializis, *IEEE Trans. Electr. Insul.* 1981, **EI–16**, 399–413.
107 H. Heywang, *Colloid Polym. Sci.*, 1976, **254**, 139–147.
108 J. H. Tortai, A. Denat and N. Bonifaci, *J. Electrostat.*, 2001, **53**, 159–169.
109 J. Kammermaier, *Frequency*, 1964, **18**, 145–150.
110 J. Kammermaier, *IEEE Trans. Electr. Insul.*, 1987, **EI–22**, 145–149.
111 H. S. Bu, S. Z. Cheng and B. Wunderlich, *Makromol. Chem. Rapid Comm.*, 1988, **9**, 75–77.
112 R. J. Plunkett, The History of Polytetrafluoroethylene: Discovery and Development, *High Performance Polymers: Their Origin and Development*, Elsevier, 1986, ch. 25.
113 P. Ehrlich, J. Res. Natl. Bur. Stand. (U. S.), 1953, **51**, 185−188.
114 J. P. Critchley, G. J. Knight and W. W. Wright, Flourine Containing Polymers, *Heat–resistant Polymers: Technologically Useful Materials*; Plenum Press, 1983, ch. 3.
115 G. Odian, *Principles of Polymerization*, John Wiley & Sons, 1991.
116 B. Wunderlich, Equilibrium Melting, *Macromolecular Physics: Crystal Melting*, Academic Press, 1980, ch. 8.

117 C. A. Sperati, Polytetrafluoroethylene: History of its Development and Some Recent Advances, *High Performance Polymers: Their Origin and Development*, Elsevier, 1986, ch. 26.

118 J. H. Cozens, *IRE Trans. Compon. Parts*, 1959, **6**, 114−118.

119 R. E. Putnam, Development of Thermoplastic Fluoropolymers, *High Performance Polymers: Their Origin and Development*, Elsevier, 1986, ch. 27.

120 J. L. Suthar and J. R. Laghari, *J. Mater. Sci.*, 1992, **2**, 1795−1800.

121 M. Donhowe, J. Lawler, S. Souffie and E. L. Stein Jr., *Add'l. Conf.*, 2011, **2011**, 000201−000206.

122 C. M. Kerwien, D. L. Malandro and J. R. Broomall, Large Area DC Dielectric Breakdown Voltage Measurement of BOPP and PTFE Thin Films, *IEEE Int'l. Conf. Electr. Insul. Dielectr. Phenomena* (*CEIDP*), IEEE, 2016.

123 S. Luo, J. Yu, T. Q. Ansari, S. Yu, P. Xu, L. Cao, H. Huang, R. Sun and C. P. Wong, *Appl. Mater. Today*, 2020, **21**, 100882.

124 S. Luo, T. Q. Ansari, J. Yu, S. Yu, P. Xu, L. Cao, H. Huang, R. Sun, *Chem. Eng. J.*, 2021, **412**, 128476.

125 Y. Takahashi, S. Ukishima, M. Iijima and E. Fukada, *J. Appl. Phys.*, 1991, **70**, 6983–6987.

126 Y. Wang, X. Zhou, M. Lin and Q. M. Zhang, *Appl. Phys. Lett.*, 2009, **94**, 202905.

127 S. Wu, W. Li, M. Lin, Q. Burlingame, Q. Chen, A. Payzant, K. Xiao, Q. M. Zhang, *Adv. Mater.*, 2013, **25**, 1734–1738.

128 S. Wu, M. Lin, Q. Burlingame and Q. M. Zhang, *Appl. Phys. Lett.*, 2014, **104**, 072903.

129 S. Wu, Q. Burlingame, Z. X. Cheng, M. Lin and Q. M. Zhang, *J. Electron. Mater.*, 2014, **43**, 4548–4551.

130 T. Zhang, X. Chen, Y. Thakur, B. Lu, Q. Zhang, J. Runt and Q. M. Zhang, *Sci. Adv.*, 2020, **6**, eaax6622.

131 B. Nandan, L. D. Kandpal and G. N. Mathur, *Polymer*, 2003, **44**, 1267–1279.

132 Y. Zhang, Z. Geng, S. Niu, S. Zhang, J. Luan and G. Wang, *Adv. Ind. Eng. Polym. Res.*, 2020, **3**, 175–185.

133 R. Wei, L. Tu, Y. You, C. Zhan, Y. Wang and X. Liu. *Polymer,* 2019, **161**, 162–169.

134 H. Tang, J. Yang, J. Zhong, R. Zhao and X. Liu, *Mater. Lett.*, 2011, **65**, 2758–2761.

135 S. Banerjee and G. Maier, *Chem. Mater.*, 1999, **11**, 2179–2184.

136 T. E. Attwood, P. C. Dawson, J. L. Freeman, L. R. J. Hoy, J. B. Rose and P. A. Staniland, *Polymer*, 1981, **22**, 1096−1103.

137 P. H. Kang, C. Lee and K. Y. Kim, *J. Ind. Eng. Chem.*, 2007, **13**, 250−256.

138 J. Pan, K. Li, J. Li, T. Hsu and Q. Wang, *Appl. Phys. Lett.*, 2009, **95**, 022902.

139 J. Pan, K. Li, S. Chuayprakong, T. Hsu and Q. Wang, *ACS Appl. Mater. Interfaces*, 2010, **2**, 1286−1289.

140 D. Xu, W. Xu, T. Seery, H. Zhang, C. Zhou, J. Pang, Y. Zhang and Z. Jiang, *Macromol. Mater. Eng.*, 2020, **305**, 1900820.

141 V. A. Bershtein, L. M. Egorova, P. N. Yakushev, P. Pissis, P. Sysel and L. Brozova, *J. Polym. Sci. B Polym. Phys.*, 2002, **40**, 1056−1069.

142 D. J. Liaw, K. L. Wang, Y. C. Huang, K. R. Lee, J. Y. Lai and C. S. Ha, *Prog. Polym. Sci.*, 2012, 37, 907−974.

143 Z. Song, H. Zhan and Y. Zhou, *Angew. Chem., Int. Ed.*, 2010, **49**, 8444−8448.

144 K. Vanherck, G. Koeckelberghs and I. F. Vankelecom, *Prog. Polym. Sci.*, 2013, 38, 874−896.

145 S. Chisca, V. E. Musteata, I. Sava and M. Bruma, *Eur. Polym. J.*, 2011, **47**, 1186−1197.

146 M. Kochi, T. Yonezawa, R. Yokota and I. Mita, Monoaxial Drawing Techniques for High Modulus/High Strength Aromatic Polyimide Films, *Advances in Polyimide Science and Technology*, CRC Press, 1993, ch. 29.

147 H. Lao, N. Mushtaq, G. Chen, H. Jiang, Y. Jiao, A. Zhang and X. Fang, *Polymer*, 2020, **206**, 122889.

148 S. Diaham and M. L. Locatelli, *J. Phys. D Appl. Phys.*, 2013, **46**, 185302.

149 S. Diaham, M. L. Locatelli, T. Lebey and S. Dinculescu, Dielectric and Thermal Properties of Polyamide-imide (PAI) Films, *IEEE Int'l. Conf. Electr. Insul. Dielectr. Phenomena* (*CEIDP*), IEEE, 2009.

150 J. Bright, Polyetherimide: High Temperature, Melt Processable Insulation, *IEEE Electr. Insul, Conf.* (*EIC*), IEEE, 1983.

151 P. Irwin, D. Tan, Y. Cao, N. Silvi, M. Carter, M. Rumler and C. Garet, *SAE Int. J. Aerosp.* 2008, **1**, 817–821.

152 B. K. Chen, J. U. Du and C. W. Hou, *IEEE Trans. Dielectr. Electr. Insul.*, 2008, **15**, 127–133.

153 C. Wu, A. A. Deshmukh, Z. Li, L. Chen, A. Alamri, Y. Wang, R. Ramprasad, G. A. Sotzing and Y. Cao, *Adv. Mater.*, 2020, **32**, 2000499.

154 F. W. MacDougall, J. Ennis, X. H. Yang, R. A. Cooper, J. E. Gilbert, J. F. Bates, C. Naruo, M. Schneider, N. Keller, S. Joshi, T. R. Jow, J. Ho, C. J. Scozzie and S. P. S Yen, *Pulsed Power Conf.*, IEEE, Piscataway NJ, USA 2009, p. 774.

155 A. Azizi, M. R. Gadinski, Q. Li, M. A. AlSaud, J. Wang, Y. Wang, B. Wang, F. Liu, L. Q. Chen, N. Alem and Q. Wang, *Adv. Mater.* 2017, **29**, 1701864.

156 Y. Wang, Z. Li, C. Wu and Y. Cao, *Chem. Eng. J.*, 2020, **401**, 126093.

157 J. T. Stricker, J. Scofield, N. Brar, J. DeCerbo, H. Kosai, T. Bixel, W. Lanter and B. Ray, *Evaluation of Fluorene Polyester Film Capacitors*, *CARTS Proceedings*, 2010.

158 N. Venkat, T. D. Dang, Z. Bai, V. K. McNier, J. N. DeCerbo, B. H. Tsao and J. T. Stricker, *Mater. Sci. Eng., B*, 2010, **168**, 16−21.

159 Y. H. So, *Prog. Polym. Sci.*, 2000, **25**, 137−157.

160 J. F. Wolfe and F. E. Arnold, *Macromolecules*, 1981, **14**, 909−915.

161 J. F. Wolfe, B. H. Loo and F. E. Arnold, *Macromolecules*, 1981, **14**, 915−920

162 L. Mandelcorn and R. L. Miller, High Temperature, >200 degrees C, Polymer Film Capacitors, *IEEE Int. Power Sources Symp.*, IEEE, 1992.

163 H. Vogel and C. S. Marvel, *J. Polym. Sci.* 1961, **50**, 511−539.

164 Q. Li, J. O. Jensen, R. F. Savinell and N. J. Bjerrum, *Prog. Polym. Sci.*, 2009, **34**, 449−477.

165 A. N. Hammoud and J. L. Suthar, Characterization of Polybenzimidazole (PBI) Film at High Temperatures, *IEEE Int. Symp. Electr. Insul*., IEEE, 1990.

166 J. R. Fried, Sub–T_g Transitions, *Physical Properties of Polymers Handbook*, Springer, 2007, ch. 13.

167 D. H. Wang, J. K. Riley, S. P. Fillery, M. F. Durstock, R. A. Vaia and L. S. Tan, *J. Polym. Sci. A Polym. Chem.* 2013, **51**, 4998–5011.

168 I. Treufeld, D. H. Wang, B. A. Kurish, L. S. Tan and L. Zhu, *J. Mater. Chem. A*, 2014, **2**, 20683–20696.

169 D. H. Wang, B. A. Kurish, I. Treufeld, L. Zhu and L. S. Tan, *J. Polym. Sci. A Polym. Chem.*, 2015, **53**, 422–436.

170 Z. Zhang, M. H. Litt and L. Zhu, *Macromolecules*, 2018, **51**, 1967–1977.

171 R. Ma, V. Sharma, A. F. Baldwin, M. Tefferi, I. Offenbach, M. Cakmak, R. Weiss, Y. Cao, R. Ramprasad and G. A. Sotzing, *J. Mater. Chem. A*, 2015, **3**, 14845–14852.

172 Z. Li, G. M. Treich, M. Tefferi, C. Wu, S. Nasreen, S. K Scheirey, R. Ramprasad, G. A. Sotzing and Y. Cao, *J. Mater. Chem. A*, 2019, **25**, 15026–15030.

173 L. Chen, C. Kim, R. Batra, J. P. Lightstone, C. Wu, Z. Li, A. A. Deshmukh, Y. Wang, H. D. Tran, P. Vashishta, G. A. Sotzing, Y. Cao and R. Ramprasad, *Npj Comput. Mater.*, 2020, **6**, 1–9.

174 X. Yin, Y. Qiao, M. R. Gadinski, Q. Wang and C. Tang, *Polym. Chem.*, 2016, **7**, 2929–2933.
175 W. L. Qu and T. M. Ko, *J. Appl. Polym. Sci.*, 2001, **82**, 1642–1652.
176 T. Yang, W. Xu, X. Peng and H. Hou, *RSC Adv.* 2017, **7**, 23309–23312.
177 X. Peng, W. Xu, L. Chen, Y. Ding, T. Xiong, S. Chen and H. Hou, *React. Funct. Polym.* 2016, **106**, 93–98.
178 X. Peng, Q. Wu, S. Jiang, M. Hanif, S. Chen and H. Hou, *J. Appl. Polym. Sci.*, 2014, **131**, 40828.
179 H. Tong, A. Ahmad, J. Fu, H. Xu, T. Fan, Y. Hou and J. Xu, *J. Appl. Polym. Sci.*, 2019, **136**, 47883.
180 H. Tong, J. Fu, A. Ahmad, T. Fan, Y. Hou and J. Xu, *Macromol. Mater. Eng.*, 2019, **304**, 1800709.
181 R. Ma, A. F. Baldwin, C. Wang, I. Offenbach, M. Cakmak, R. Ramprasad and G. A. Sotzing, *ACS Appl. Mater. Interfaces*, 2014, **6**, 10445–10451.
182 F. Wen, L. Zhang, P. Wang, L. Li, J. Chen, C. Chen, W. Wu, G. Wang and S. Zhang, *J. Mater. Chem. A*, 2020, **8**, 15122–15129.
183 J. T. Bendler, D. A. Boyles, C. A. Edmondson, T. Filipova, J. J. Fontanella, M. A. Westgate and M. C. Wintersgill, *Macromolecules*, 2013, **46**, 4024–4033.
184 J. Wei, Z. Zhang, J. K. Tseng, I. Treufeld, X. Liu, M. H. Litt and L. Zhu, *ACS Appl. Mater. Interfaces*, 2015, **7**, 5248–5257.
185 Y. Zhu, Z. Zhang, M. H. Litt and L. Zhu, *Macromolecules*, 2018, 51, 6257–6266.
186 J. Wei, T. Ju, W. Huang, J. Song, N. Yan, F. Wang, A. Shen, Z. Li and L. Zhu, *Polymer*, 2019, **178**, 121688.
187 Z. Zhang, D. H. Wang, M. H. Litt, L. S. Tan and L. Zhu, *Angew. Chem., Int. Ed.*, 2018, **57**, 1528–1531.
188 N. Du, G. P. Robertson, I. Pinnau and M. D. Guiver, *Macromolecules*, 2009, **42**, 6023–6030.
189 Z. Zhang, J. Zheng, K. Premasiri, M. H. Kwok, Q. Li, R. Li, S. Zhang, M. H. Litt, X. P. A. Gao and L. Zhu, *Mater. Horiz.*, 2020, **7**, 592–597.
190 I. Pleşa, P. V. Noţingher, S. Schlögl, C. Sumereder and M. Muhr, *Polymers*, 2016, **8**, 173.
191 Y. Lin, X. Huang, J. Chen and P. Jiang, *High Volt.*, 2017, **2**, 139–146.
192 R. A. Pearson and A. F. Yee, *J. Mater. Sci.*, 1989, **24**, 2571–2580.
193 H. B. Wang, Y. G. Yang, H. H. Yu, W. M. Sun, Y. H. Zhang and H. W. Zhou, *Polym. Eng. Sci.*, 1995, **35**, 1895–1898.
194 A. K. Sadana, R. K. Saini and W. E. Billups, *Chem. Rev.*, 2003, **103**, 1539–1602.
195 T. L. Hanley, R. P. Burford, R. J. Fleming and K. W. Barber, *IEEE Electr. Insul. Mag.*, 2003, **19**, 13–24.
196 Y. Xie, Y. Yu, Y. Feng, W. Jiang and Z. Zhang, *ACS Appl. Mater. Interfaces*, 2017, **9**, 2995–3005.
197 X. Wang, B. Qiao, S. Tan, W. Zhu and Z. Zhang, *J. Mater. Chem. C*, 2020, **8**, 11426–11440.
198 P. Khanchaitit, K. Han, M. R. Gadinski, Q. Li and Q. Wang, *Nat. Commun.*, 2013, **4**, 2845.
199 H. Li, M. R. Gadinski, Y. Huang, L. Ren, Y. Zhou, D. Ai, Z. Han, B. Yao and Q. Wang, *Energy Environ. Sci.*, 2020, **13**, 1279–1286.
200 Y. You, S. Liu, L. Tu, Y. Wang, C. Zhan, X. Du, R. Wei and X. Liu, *Macromolecules*, 2019, **52**, 5850–5859.
201 Y. Zhang, Z. Liu, L. Zhu, J. Liu, Y. Zhang and Z. Jiang, *CCS Chem.*, 2020, **2**, 1169–1177.
202 Q. Li and Q. Wang, *Macromol. Chem. Phys.*, 2016, **217**, 1228–1244.
203 L. Zhu, *J. Phys. Chem. Lett.*, 2014, **5**, 3677–3687.
204 Y. Feng, Y. Hasegawa, T. Suga, H. Nishide, L. Yang, G. Chen and S. Li, *Macromolecules*, 2019, **52**, 8781–8787.
205 Y. Thakur, B. Zhang, R. Dong, W. Lu, C. Iacob, J. Runt, J. Bernholc and Q. M. Zhang, *Nano Energy*, 2017, **32**, 73–79.
206 Q. Zhang, X. Chen, T. Zhang and Q. M. Zhang, *Nano Energy*, 2019, **64**, 103916.
207 C. Yuan, Y. Zhou, Y. Zhu, J. Liang, S. Wang, S. Peng, Y. Li, S. Cheng, M. Yang, J. Hu, B. Zhang, R. Zeng, J. L. He and Q. Li, *Nat. Commun.*, 2020, **11**, 3919.
208 M. Jarvid, A. Johansson, R. Kroon, J. M. Bjuggren, H. Wutzel, V. Englund, S. Gubanski, M. R. Andersson and C. Müller, *Adv. Mater.*, 2015, **27**, 897–902.
209 H. Yuan, Y. Zhou, Y. Zhu, S. Hu, C. Yuan, W. Song, Q. Shao, Q. Zhang, J. Hu, Q. Li and J. L. He, *J. Phys. D Appl. Phys.*, 2020, **53**, 475301.
210 E. Baer and L. Zhu, *Macromolecules*, 2017, **50**, 2239–2256.
211 X. Chen, J. K. Tseng, I. Treufeld, M. Mackey, D. E. Schuele, R. Li, M. Fukuto, E. Bear and L. Zhu, *J. Mater. Chem. C*, 2017, **5**, 10417–10426.
212 M. Mackey, D. E. Schuele, L. Zhu, L. Flandin, M. A. Wolak, J. S. Shirk, A. Hiltner and E. Baer, *Macromolecules*, 2012, **45**, 1954–1962.
213 Z. Li, X. Chen, C. Zhang, E. Baer, D. Langhe, M. Ponting, M. Brubaker, T. Hosking, R. Li, M. Fukuto and L. Zhu, *ACS Appl. Polym. Mater.*, 2019, **1**, 867–875.
214 X. Chen, Q. Li, D. Langhe, M. Ponting, R. Li, M. Fukuto, E. Baer and L. Zhu, *ACS Appl. Mater. Interfaces*, 2020, **12**, 44892–44901.
215 J. M. Carr, M. Mackey, L. Flandin, D. Schuele, L. Zhu and E. Baer, *J. Polym. Sci. B Polym. Phys.*, 2013, **51**, 882–896.
216 J. K. Tseng, S. Tang, Z. Zhou, M. Mackey, J. M. Carr, R. Mu, L. Flandin, D. E. Schuele, E. Baer and L. Zhu, *Polymer*, 2014, **55**, 8–14.
217 K. Yin, J. Zhang, Z. Li, J. Feng, C. Zhang, X. Chen, A. Olah, D. E. Schuele, L. Zhu and E. Baer, *J. Appl. Polym. Sci.*, 2019, **136**, 47535.
218 H. Huang, X. Chen, K. Yin, I. Treufeld, D. E. Schuele, M. Ponting, D. Langhe, E. Baer and L. Zhu, *ACS Appl. Energy Mater.*, 2018, **1**, 775–782.
219 G. Liu, T. Zhang, Y. Feng, Y. Zhang, C. Zhang, Y. Zhang, X. Wang, Q. Chi, Q. Chen and Q. Lei, *Chem. Eng. J.*, 2020, **389**, 124443.

Table of contents entry

The electrification of transport and growing demand for advanced electronics require polymer dielectrics capable of operating efficiently at high temperatures. The development of high-temperature dielectric polymers is reviewed from the perspective of structure design, dielectric properties and capacitive performance.

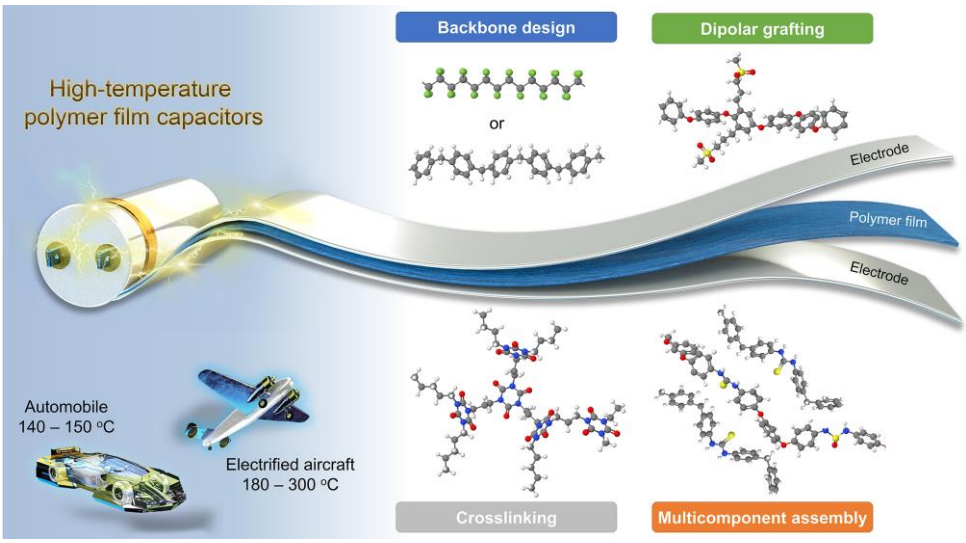

Table 1 Comparison of key physical parameters of dielectric polymers for high-temperature capacitive energy storage.

Polymer	Dielectric constant	Dissipation factor	Dielectric breakdown strength (MV m^{-1})	Maximum discharged energy density (J cm^{-3})	Charge–discharge efficiency (%)	Glass transition temperature (°C)	Ratio of (C + N + S) to (H + O)	Electrode area (mm^2)	Film thickness (μm)	Ref.
BOPP	~ 2.25 @ 20 °C and 1 kHz	~ 0.01% @ 20 °C and 1 kHz	496 @ 120 °C	1.28 @ 120 °C and 10 Hz	52.1 @ 120 °C and 10 Hz	< 0	0.5	9.62	5.8	17
PC	~ 3 @ 25 °C and 1 kHz	~ 0.1% @ 25 °C and 1 kHz	/	1.29 @ 150 °C and 10 Hz	47 @ 150 °C and 10 Hz	~ 150–160	0.94	9.62	10	17
PPS	~ 3–3.1 @ 25 °C and 1 kHz	~ 0.3% @ 25 °C and 1 kHz	/	0.22 @ 150 °C and 10 Hz	57.4 @ 150 °C and 10 Hz	~ 90	1.75	9.62	6	17
PET	~ 3 @ 25 °C and 1 kHz	~ 0.2% @ 25 °C and 1 kHz	/	0.93 @ 150 °C and 10 Hz	58 @ 150 °C and 10 Hz	~ 70–80	0.83	9.62	3.5	17
PEN	~ 2.9–3 @ 25 °C and 1 kHz	~ 0.1–0.2% @ 25 °C and 1 kHz	/	1.41 @ 150 °C and 10 Hz	68.8 @ 150 °C and 10 Hz	~ 125	1	9.62	4	17
Kapton® PI	~ 3.3–3.4 @ 25 °C and 1 kHz	~ 0.1% @ 25 °C and 1 kHz	314 @ 150 °C	0.82 @ 150 °C and 10 Hz	55.7 @ 150 °C and 10 Hz	~ 360	1.6	5.31	9–12	6, 61
Ultem® PEI	~ 3.2 @ 25 °C and 1 kHz	~ 0.1% @ 25 °C and 1 kHz	439 @ 150 °C	1.6 @ 150 °C and 10 Hz	33.7 @ 150 °C and 10 Hz	~ 217	1.3	5.31	8–14	6, 67
FPE	~ 3.5 @ 25 °C and 1 kHz	~ 0.1% @ 25 °C and 1 kHz	/	1.2 @ 150 °C and 10 Hz	40.8 @ 150 °C and 10 Hz	~ 330	1.32	28.26	6	6
PTFE	~ 2.17 @ 25 °C and 1 kHz	~ 0.15% @ 25 °C and 1 kHz	350 @ 200 °C	1.08 @ 200 °C and 100 Hz	94 @ 200 °C and 100 Hz	/	/	4.91	4–5	123
PTFE with epoxy coating	~ 2.28 @ 25 °C and 1 kHz	~ 0.2–0.6% @ 25 °C and 1 kHz	392 @ 150 °C	1.93 @ 150 °C and 100 Hz	98.9 @ 150 °C and 100 Hz	/	/	78.5	6–7	124
ArPU	~ 4.2 @ 25 °C and 1 kHz	~ 0.5% @ 25 °C and 1 kHz	> 500 @ 180 °C	~ 6 @ 180 °C and 1 kHz	~ 50 @ 180 °C and 1 kHz	/	1.23	/	~ 2.5	126
ArPTU	~ 4.5 @ 25 °C and 1 kHz	~ 1% @ 25 °C and 1 kHz	~ 1000 @ 25 °C	22 @ 25 °C and 10 Hz	~ 92 @ 25 °C and 10 Hz	/	1.42	3.14 or 28.26	1–5	127
PEEU	4.7 @ 25 °C and 1 kHz	~ 0.15% @ 25 °C and 1 kHz	400 @ 150 °C	2.9 @ 150 °C and 10 Hz	~ 74 @ 150 °C and 10 Hz	> 250	1.24	4.52	2–3	130

PEKK	3.6 @ 25 °C and 1 kHz	~ 0.3% @ 25 °C and 1 kHz	420 @ 140 °C	2.37 @ 140 °C and 100 Hz	~ 35 @ 140 °C and 100 Hz	155	1.33	5.31	~ 25	138
PPEK	3.5 @ 25 °C and 1 kHz	0.63% @ 25 °C and 1 kHz	441 @ 190 °C	2.1 @ 190 °C and 100 Hz	~ 44 @ 190 °C and 100 Hz	~ 250	1.53	5.31	20–40	139
ht-PEKNA	5.3 @ 25 °C and 1 kHz	~ 1% @ 25 °C and 1 kHz	> 350 @ 200 °C	2.9 @ 200 °C and 100 Hz	~ 50 @ 200 °C and 100 Hz	~ 251	1.34	9.62	5–15	140
POFNB	2.5 @ 25 °C and 1 kHz	< 0.5% @ 25 °C and 1 kHz	~ 650 @ 150 °C	~ 5.7 @ 150 °C and 100 Hz	~ 78 @ 150 °C and 100 Hz	186	/	7.07	~ 10	153
ABS	4.6 @ 30 °C and 1 kHz	~ 2% @ 30 °C and 1 kHz	480 @ 120 °C	6.7 @ 120 °C and 10 Hz	75 @ 120 °C and 10 Hz	128	1	/	~ 15	182
SO_2-PPO_{25}	5.9 @ 25 °C and 1 kHz	~ 0.6% @ 25 °C and 1 kHz	/	2.24 @ 150 °C and 1 kHz	78.9 @ 150 °C and 1 kHz	228	/	4.52	3–8	187
SO_2-PPO_{52}	8.2 @ 25 °C and 1 kHz	~ 0.9% @ 25 °C and 1 kHz	/	3.06 @ 100 °C and 1 kHz	72.6 @ 100 °C and 1 kHz	211	/	4.52	3–8	187
SO_2-PIM	~ 5.3 @ 40 °C and 1 kHz	~ 0.5% @ 40 °C and 1 kHz	/	~ 2.32 @ 150 °C and 1 kHz	~ 93 @ 150 °C and 1 kHz	≥ 350	0.92	4.52	0.2–8	189
Epoxy resin	~ 4.4 @ 25 °C and 1 kHz	~ 1.3% @ 25 °C and 1 kHz	610 @ 25 °C	~ 1 @ 120 °C and 100 Hz	~ 90 @ 120 °C and 100 Hz	150	0.67	3.14	12	104
XL-VK	3.19 @ 25 °C and 1 kHz	~ 2.5% @ 25 °C and 1 kHz	494 @ 150 °C	4.33 @ 150 °C and 10 Hz	70 @ 150 °C and 10 Hz	/	/	5.31	10–20	199
c-PAEN	3.79 @ 25 °C and 1 kHz	1.6% @ 25 °C and 1 kHz	188 @ 300 °C	0.8 @ 150 °C and 1 kHz	/	~ 370	/	/	/	200
c-PEPA-PEI	~ 2.9 @ 25 °C and 1 kHz	~ 0.37% @ 25 °C and 1 kHz	~ 500 @ 150 °C	3.6 @ 150 °C and 100 Hz	96.5 @ 150 °C and 100 Hz	~ 210–220	/	78.5	~ 20	201
PEI/PCBM	~ 3.25% @ 25 °C and 1 kHz	~ 0.2% @ 25 °C and 1 kHz	649 @ 200 °C	~ 3.2 @ 200 °C and 10 Hz	~ 88 @ 200 °C and 10 Hz	~ 217	/	7.07	10–12	207

Note: The charge–discharge efficiencies were obtained at the same electric field of the maximum discharged energy density.

BOPP: biaxially-oriented polypropylene; PC: polycarbonate; PPS: poly(phenylene sulfide); PET: poly(ethylene terephthalate); PEN: poly(ethylene terephthalate); PI: polyimide; PEI: polyetherimide; FPE: fluorene polyester; PTFE: Polytetrafluoroethylene; ArPU: aromatic polyurea; ArPTU: aromatic polythiourea; PEEU: poly(arylene ether urea); PEKK: poly(ether ketone ketone); PPEK: poly(phthalazinone ether ketone); ht-PEKNA: heat-annealed poly(naphthalene ether ketone amide); POFNB: polyoxafluoronorbornene; ABS: poly(acrylonitrile-*co*-butadiene-*co*-styrene); SO_2-PPO: sulfonylated poly(2,6-dimethyl-1,4-phenylene oxide); SO_2-PIM: sulfonylated polymers of intrinsic microporosity; XL-VK: crosslinked

poly(chlorotrifluoroethylene-*co*-vinylidene fluoride); *c*-PAEN: crosslinked poly(aryl ether nitrile); *c*-PEPA-PEI: crosslinked 4-phenylethynylphthalic anhydride-terminated polyetherimide; PEI/PCBM: polyetherimide filled with [6,6]-phenyl C61 butyric acid methyl ester